Effects of increase glacier discharge on phytoplankton bloom dynamics and pelagic geochemistry in a high Arctic fjord

Maria Ll. Calleja, P. Kerhervé, S. Bourgeois, M. Kędra, Aude Leynaert, E. Devred, M. Babin, N. Morata

Effects of increase glacier discharge on phytoplankton bloom dynamics and pelagic geochemistry in a high Arctic fjord

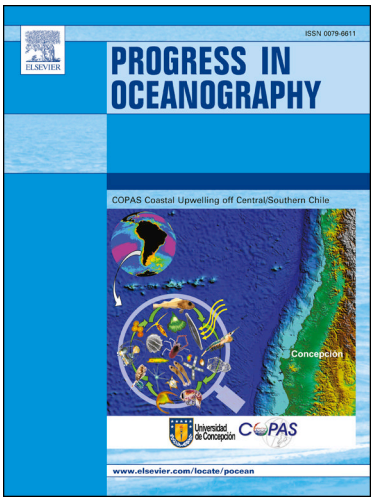

Effects of increase glacier discharge on phytoplankton bloom dynamics and pelagic geochemistry in a high Arctic fjord

Maria Ll. Calleja, P. Kerhervé, S. Bourgeois, M. Kędra, A. Leynaert, E. Devred, M. Babin, N. Morata

PII: S0079-6611(16)30180-X
DOI: http://dx.doi.org/10.1016/j.pocean.2017.07.005
Reference: PROOCE 1828

To appear in: *Progress in Oceanography*

Received Date: 9 September 2016
Revised Date: 12 July 2017
Accepted Date: 18 July 2017

Please cite this article as: Calleja, M.L., Kerhervé, P., Bourgeois, S., Kędra, M., Leynaert, A., Devred, E., Babin, M., Morata, N., Effects of increase glacier discharge on phytoplankton bloom dynamics and pelagic geochemistry in a high Arctic fjord, *Progress in Oceanography* (2017), doi: http://dx.doi.org/10.1016/j.pocean.2017.07.005

Effects of increase glacier discharge on phytoplankton bloom dynamics and pelagic geochemistry in a high Arctic fjord

Maria Ll. Calleja[1,2*], Kerhervé, P[3], Bourgeois, S[4,5], Kędra, M[6], Leynaert, A[4], Devred, E[7], Babin, M[7] and Morata, N[4]

[1]Instituto Andaluz de Ciencias de la Tierra. IACT (CSIC–UGR), Avenida de Las Palmeras 4, 18100 Armilla, Granada, Spain.

[2]King Abdullah University of Science and Technology, Thuwal 23955-6900, Saudi Arabia.

[3]Centre de Formation et de Recherche sur les Environnements Méditerranéens (CEFREM), UMR5110, Université de Perpignan Via Domitia, 66860, Perpignan, France.

[4]Laboratoire des sciences de l'Environnement MARin (LEMAR), UMR 6539, Université de Bretagne Occidentale, Rue Dumont D'Urville, 29280 Plouzané, France.

[5]School of Biological Sciences, Oceanlab, University of Aberdeen, Aberdeen, Scotland AB41 6AA, UK

[6]Institute of Oceanology, Polish Academy of Sciences, Powstańców Warszawy 55, Sopot 81-712, Poland.

[7]Takuvik, UMI 3316, Université Laval, Département de Biologie, Pavillon Alexandre-Vachon 1045, avenue de la Médecine, Québec City, QC G1V 0A6, Canada

* corresponding author current address: King Abdullah University of Science and Technology, Thuwal 23955-6900, Saudi Arabia. e-mail: maria.callejacortes@kaust.edu.sa

Abstract

Arctic fjords experience extremely pronounced seasonal variability and spatial heterogeneity associated with changes in ice cover, glacial retreat and the intrusion of continental shelf's adjacent water masses. Global warming intensifies natural environmental variability on these important systems, yet the regional and global effects of these processes are still poorly understood. In the present study, we examine seasonal and spatial variability in Kongsfjorden, on the western coast of Spitsbergen, Svalbard. We report hydrological, biological, and biogeochemical data collected during spring, summer, and fall 2012. Our results show a strong phytoplankton bloom with the highest chlorophyll *a* (Chl*a*) levels ever reported in this area, peaking 15.5 µg/L during late May and completely dominated by large diatoms at the inner fjord, that may sustain both pelagic and benthic production under weakly stratified conditions at the glacier front. A progressively stronger stratification of the water column during summer and fall was shaped by the intrusion of warm Atlantic water (T > 3ºC and Sal > 34.65) into the fjord at around 100 m depth, and by turbid freshwater plumes (T < 1ºC and Sal < 34.65) at the surface due to glacier meltwater input. Biopolymeric carbon fractions and isotopic signatures of the particulate organic material (POM) revealed very fresh and labile material produced during the spring bloom (^{13}C enriched, with values up to -22.7‰ at the highest Chl *a* peak, and high in carbohydrates and proteins content -up to 167 and 148 µg/L, respectively-), and a clear and strong continental signature of the POM present during late summer and fall (^{13}C depleted, with values averaging -26.5 ‰, and high in lipid content –up to 92 µg/L-) when freshwater melting is accentuated. Our data evidence the importance of combining both physical (i.e. water mass dominance) and geochemical (i.e. characteristics of material released by glacier runoff) data in order to understand the timing, intensity and characteristics of the phytoplankton bloom in

Kongsfjorden, a continuously changing system due to sustained warming. In a scenario where glacial retreat is predicted to increase the impacts of meltwater discharge and associated delivery of organic and inorganic material to the surrounding waters, special attention is required in order to predict the consequences for Arctic fjords and adjacent shelf ecosystems.

Keywords: Arctic, fjords, glaciers, organic matter, diatom bloom, carbon and nitrogen stable isotopes

Regional index terms: Norway, Svalbard, Spitsbergen, Kongsfjorden

1. Introduction

Climate change is strongly affecting high latitude regions due to rapid alterations in the sea ice cover, with consequences on local and global weather patterns and biogeochemical cycles (Stroeve et al. 2005). On a regional and coastal scale, the effects of sea ice cover reduction in the Arctic are strongly amplified by glacier retreat (Pritchard et al. 2009). Predictions are that warming and retreat of sea ice cover and glaciers will most likely involve shifts in arctic marine ecosystem, from the predominance of benthic communities and bottom-feeding organisms (in a traditional ice abundant Arctic scenario where high biomass of algae are exported to the benthos) to a living community more dominated by pelagic fish (in an ice-free scenario where light penetration stimulates pelagic blooms and zooplankton grazing) (Grebmeier et al. 2006, Kędra et al. 2015).

Poorly studied but singularly important are the effects of changes in the heterogeneous biogeochemical material, incorporated in glaciers during different time scales (Hood et al. 2015), that is being released in seawater due to increasing glacial melt (e.g. macro-nutrients, iron, organic matter, sediments, etc.). Glaciers are also known to be biologically active, containing microorganisms that can produce or degrade organic compounds and sequester nitrogen from the atmosphere thus playing a potential key role in the carbon and nitrogen cycles (Telling et al. 2011, Grzesiak et al. 2015). However many questions still remain on the origin, nature and fate of the material released to the water column through increasing glacial melt, which is critical to understand the mechanisms that sustain and/or threaten life in the surrounding ecosystem.

Glaciers from the west coast of Spitsbergen, the largest island of the high Arctic archipelago of Svalbard (74 to 81º N, 10 to 35º E), are shrinking and retreating at rates ranging from 10 to 220

meters per year (Rachlewicz et al. 2007) with intrinsic consequences on ecosystem functioning including marine productivity patterns and biogeochemical cycles (Doney et al. 2012). Glacial retreat in this region is amplified by the influence of increased inflow of relatively warm Atlantic Water (AW) through the Fram Strait and the Barent Sea (Schauer et al. 2004, Polyakov et al. 2005, Piechura and Walczowski 2009, Walczowski 2013). Atlantic water forms an intermediate layer as it subducts below colder, fresher and less dense Arctic Waters (ArW). In Svalbard the balance between relatively warm AW carried northwards by the West Spitsbergen Current (WSC), cold ArW carried southward by the East Greenland Current (EGC) and recirculated towards Svalbard, and freshwater continental inputs due to glacier ice melt can be a sensitive indicator of environmental changes (Cokelet et al. 2008). As such, Svalbard fjords are particularly suitable sites to study changes on ecosystem functioning related to glacier melting in a global warming scenario (Svendsen et al. 2002).

The present study was conducted in Kongsfjorden, an open fjord on the West Spitsbergen Shelf, influenced by relatively warm AW and retreating tidewater glaciers. In the last decades, the fjord system has experienced increased summer and winter temperatures (Walczowski 2013), leading to a drastic reduction in sea ice coverage during the winter (Hop et al. 2006, Skirbekk et al 2010), and a more maritime climate throughout the year. Increased heat flux into Kongsfjorden resulting from AW inflow exerts a direct influence on the abundance, distribution and composition of the phytoplankton community (Wang et al. 2009, Hodal et al. 2012, Hegseth and Tverberg 2013) and on the microbial food web of the pelagic realm (Iversen and Seuthe 2011), with direct trophic cascade effects on both the pelagic and benthic ecosystems (Kędra et al. 2012). In particular, Hegseth and Tverberg (2013) may have identified climate-related changes in documenting a shift in phytoplankton bloom timing and duration as well as a change in commu-

nity composition compared to observations collected 20 years prior to 2006. However, a number of studies from the last decade are inconclusive displaying high variations in bloom timing and intensity (e.g. Hegseth and Tverberg 2008, Kubiszyn et al 2014).

Several aspects of physical changes on the marine system remain uncertain. Glacial run-off decreases the salinity of the upper water column, and enhances the transport of glacial material into the inner fjord creating steep environmental gradients in the fjord system (e.g., Grotti et al. 2013; Frankowski and Ziola-Frankowska 2014). Yet only scarce data exist on the role organic and mineral glacier inputs play into Kongsfjorden ecosystem (Svendsen et al. 2002) making it difficult to predict bloom conditions.

In this study, we implemented a spatially and temporally explicit sampling strategy to provide new information on hydrological, biological, and geochemical variability within the waters of Kongsfjorden during 2012, a particularly warm and reduced-ice year in the entire Arctic (Hansen et al. 2014, Krishfield et al. 2014, Hawkings et al. 2015). The first goal of this work was to characterize seasonal hydrographic patterns within the fjord and seasonality in phytoplankton biomass and community composition. This was done by measuring seasonal changes in temperature, salinity, stratification and nutrients, alongside quantification of phytoplankton community composition and water mass distribution within the fjord. The second goal was to quantify and characterize the magnitude and nature of the material occurring in the water column and identify its potential sources. This was accomplished by examining a combination of biogeochemical indicators such as chloropigments, carbon and nitrogen stable isotopic composition, optical properties, and analysis of the biopolymeric carbon fractions (proteins, lipids and carbohydrates).

To the best of our knowledge, this is the first integrative study that concurrently analyzes physical, geochemical and biological water column properties in a seasonal and spatial scale in

Kongsfjorden. It includes hydrographic patterns, biogeochemical descriptions and a detailed analysis of the sources of organic matter. Our interdisciplinary work sheds light on the combined impacts of increasing Atlantic water intrusion and glacier melt on the fjord ecosystem. Taken together, these new insights will improve understanding of the potential effects of climate change on Svalbard Arctic fjords that are important mixing zones between marine and terrestrial systems.

2. Materials and methods

2.1. Study site

Kongsfjorden is a medium-sized fjord on the northwest coast of Spitsbergen (79º N, 12º E, Svalbard archipelago, see Fig. 1). This fjord is oriented from south-east to north-west, and is 27 km long, varying in width from 4 km at its head to 10 km at its mouth (Svendsen et al. 2002). The total fjord area was estimated as 208.8 km^2 and the volume as 29.4 km^3 (Ito and Kudoh 1997). Water depth in the inner part of the fjord is relatively shallow (less than 100 m depth), gets deeper at its central fjord basin, and reaches the deepest point (394 m) at the outer basin where the fjord opens to the marine water masses across the West Spitsbergen Shelf. Rather than a sill in the mouth, there is a prominent trench (Svendsen et al. 2002). The inner part is separated from the main fjord by a chain of islands (Lovénøyane) and is seasonally influenced by meltwater exports from four retreating tidewater glaciers (150 m y^{-1}, Svendsen et al. 2002). In the absence of melting sea ice cover for the last decade (Kortsch et al. 2012) marine terminating glaciers have become the main source of meltwater to Kongsfjorden (MacLachlan et al. 2007). Although there are high inter-annual variability in the timing of onset of glacial melt, it usually

starts in April and peaks in July and discharges about 1 km^3 (which represents about 3.4% of the total fjord volume) of freshwater into the inner and central fjord (Svendsen et al. 2002).

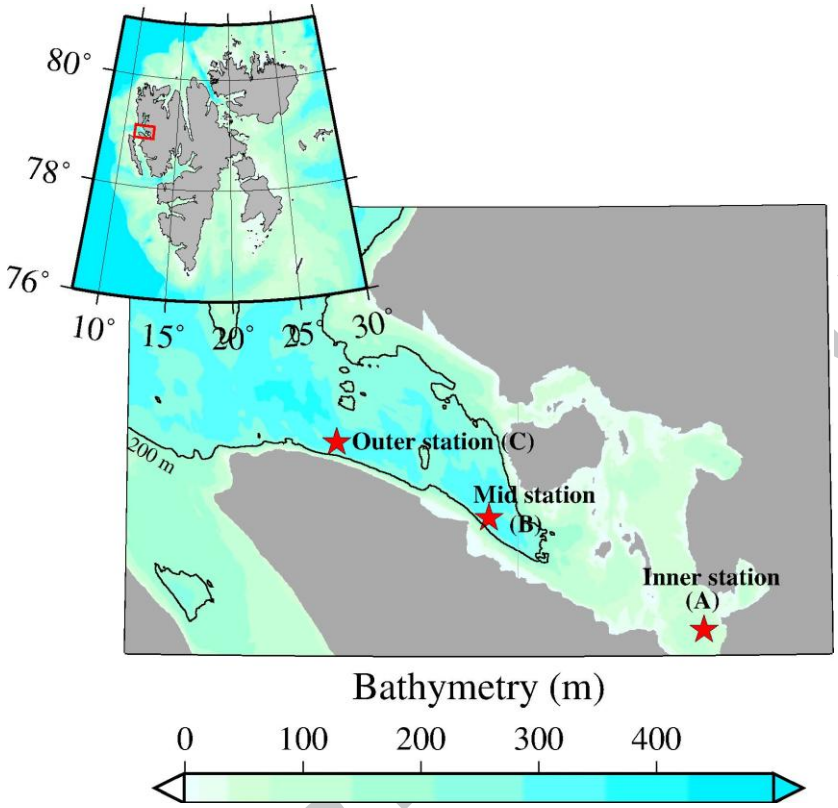

Figure1. Map of Svalbard (Norway) and Kongsfjorden, including the location of sampled stations and the fjord's bathymetry. Bathymetric data were obtained from the Norwegian Mapping Authority: Kartverket (www.kartverket.no)

A summary of water mass properties of Kongsfjorden and the adjacent shelf appears in Table 1. The relatively warm and saline AW is particularly pronounced during midsummer whereas the colder and fresher ArW gradually replaces AW in the fjord through the fall and winter (Svendsen

et al 2002, Cottier et al. 2005). The mixing of AW and ArW in Kongsfjorden forms the Transformed Atlantic Water (TAW), characterized by temperature and salinity properties distinct from water in the core of WSC. During spring and early summer the air temperature increase and freshwater from melting glaciers forms a layer of surface water (SW). That generates a vertical stratification in the fjord basin. The front separating the fjord and shelf water weakens, allowing the advection of Atlantic water types (AW and TAW) to penetrate into the fjord. Mixing between SW and the underlying Atlantic water types produces a layer of intermediate water (IW). As a consequence the fjord shifts from an ArW ti an AW (ArW) dominated system (Svendsen et al. 2002, Hop et al. 2006). The water column is well stratified in the summer. In fall and winter, winter cooled water (WCW) is formed within the fjord with temperatures lower than 1ºC and close to freezing point. By the end of the winter, WCW remains relatively homogeneous within the fjord, and can persist in the fjord basin throughout the year.

		Characteristics		
Water mass	**Abbreviation**	**T (°C)**	**Sal**	**σ_0 (Kg/m^3)**
Surface Water	SW	> 1	< 34	
Intermediate Water	IW	> 1	34 to 34.65	
Transformed Atlantic Water	TAW	1 to 3	> 34.65	< 27.92
Atlantic Water	AW	> 3	> 34.65	< 27.92
Arctic Water	ArW	-1.5 to 1	34.3 - 34.8	
Winter Cooled Water	WCW	< -0.5	34.4 to 35	

Table 1. Abbreviations and characteristics of the water mass constituents of Kongsfjorden and adjacent shelf. These domains are represented in the T-S diagram of Figure 3.

Primary production in Kongsfjorden is dependent on light, nutrient availability, stratification, and mixing. The depth of the euphotic layer decreases from a maximum of 30 m at the fjord entrance to 0.3 m in the turbid waters close to the glacier fronts. The summer season is characterized by diverse phytoplankton communities, with more than 130 taxa recorded (Piwosz et al. 2009). Dinoflagellates have been documented as the dominating microalgal groups in the inner part of the fjord, while chrysophytes and diatoms dominate the middle and outer part, respectively (Hop et al. 2002, Piwosz et al. 2009, 2015, Kubiszyn et al. 2014). Strong environmental gradients in sedimentation and seasonal freshwater inputs induce large differences in microbial and faunal community composition and abundance from the inner to outer fjord, particularly for the benthos (e.g., Holte et al 1996, Holte and Gulliksen 1998, Włodarska-Kowalczuk et al. 2004, 2005, Bourgeois et al. 2016).

2.2. Sampling strategy

Sampling was conducted at three stations during three seasons in 2012, under the umbrella of Effect of Climate Change On The Arctic Benthos ECOTAB program. Sampling periods included spring (18th to 26th of May; ECOTAB1), summer (1st to 9th of August; ECOTAB2) and fall (2nd to 13th of October; ECOTAB3) campaigns. Stations were distributed along a gradient from the inner-tidewater glacier to the ocean (Fig. 1). Inner-fjord (A) station (78°53.528 N, 12°28.413 E, 80 m deep) was located 1.4 km from the head of the fjord under the direct influence of the tidewater glacier inputs. The middle-fjord (B) station (78°56.857 N, 11°55.587 E, 295 m deep) was located midway between the tidewater glacier and the ocean. The outer (C) station

(78°59.074 N, 11°32.138 E, 305 m deep) was located 24 km from the head of the fjord, near the fjord mouth.

Air temperature (Air T, ºC) and downwelling incident photosynthetically active radiation (PAR, W m^{-2}) were continuously acquired at the meteorological station of the nearby scientific village of Ny-Ålesund, using the equipment maintained by the Alfred Wegener Institute and Paul Emile Victor (AWIPEV) polar and marine research base. Daily and fieldwork-period means of air temperature and PAR were calculated using a one-minute resolution. A SeaBird® SBE XR-620 CTD system was deployed 21 times during the three fieldwork periods, always prior to every biological and geochemical sampling. Water temperature (T, ºC), salinity (Sal, S.I.) and chlorophyll *a* fluorescence (Fluor, µg/L) were recorded in all depth profiles and used to analyze the hydrological conditions of the fjord basin during the different sampling periods. In order to validate the fluorescence data, a Spearman's rank correlation was performed between the concentrations of chlorophyll *a* extracted from the discrete samples taken (Chl*a*, µg/L) and the values recorded by the fluorometer (Fluor) (Fluor= 1.1 x Chl*a*, r=0.99, N=30). Although we observed the fluorescence measurements from the CTD sensor to be on average 0.053 µg/L lower than Chl*a* values measured from discrete samples, the two data sets did not show statistically significant differences (Kolmogorov–Smirnov KS Test, $p > 0.5$). Therefore we consider Fluor data equivalent to Chl*a* data and express it in µg/L.

In addition, the buoyancy frequency, also known as the Brünt-Väisälä frequency, N^2 (s^{-1}), was calculated according to the following equation:

$$N^2 = -\frac{g}{\rho}\frac{d\rho}{dz}$$

where g is the gravity (9.81 m s^{-2}), ρ is the potential density (kg m^{-3}) and z the depth (m). N^2 and computed using the function *swN2()* from the R oce package

(http://dankelley.github.io/oce/) as a measure for the strength of stratification. In brief, positive buoyancy indicates a stable water mass. High value of N^2 near the surface indicates a strong stratification with a shallow mixed layer depth.

Discrete samples were collected per triplicate in GoFlo® bottles for biological and geochemical analysis at each station during each sampling period. Three depths were sampled at Station A (surface, maximum Chl*a* fluorescence and bottom), while four depths were sampled at Stations B and C (surface, maximum Chl*a* fluorescence, intermediate and bottom). Water from each sample was analysed for: dissolved inorganic nutrients, to evaluate the nutrients available for primary production; chloropigments, to study biomass (Chl*a*) and degradation pigment signatures (pheopigments); phytoplankton identification and enumeration, to determine the phytoplankton major groups; biogenic silica, to quantify silica cycling relative to diatom abundance; particulate organic carbon and nitrogen, to quantify organic matter; protein, lipid and carbohydrate fractions to evaluate the varying quality of organic matter for potential grazers and sediment deposition; carbon and nitrogen stable isotopes ($\delta^{13}C$ and $\delta^{15}N$), indicative of material source (i.e. terrestrial *vs* marine); and optical properties of the dissolved organic carbon, as complementary information on the organic carbon origin.

2.3. Analytical methods

2.3.1. Dissolved inorganic nutrients

Samples for nutrient analyses were filtered through 0.2 µm Millipore® polycarbonate filters and filtrates were stored frozen at -20 ºC until analysis, except samples for silicate analyses that were stored at 4 ºC. Analysis were performed according to Aminot and Kérouel (2007). Briefly, nitrate (NO_3^-), nitrite (NO_2^-), silicate ($Si(OH)_4$) and phosphate (PO_4^{3-}) were analyzed by colorimetry on

a Bruan and Luebbe® Autoanalyzer 3HR, while ammonium (NH_4^+) was analyzed by fluorimetry. Analytical precision for all analyses was 0.05 µmol/L. All reagents and standards were prepared in acid-washed glassware, and standards were prepared with a nutrient-free artificial seawater matrix at the laboratory.

2.3.2. Chlorophyll a, pheopigments and biogenic silica

Samples for pigment and biogenic silica analyses were collected by gently filtering between 100 and 1000 mL of seawater from each sample. For pigments, Whatman® glass fiber filters (GF/F) were used and kept frozen at -80ºC in darkness. Once at the laboratory, the filters were placed in tubes with a 90% acetone solution to extract pigments, and held for 24 h in darkness at 4 ºC. Samples were then measured on a Turner® Designs model 10-AU fluorometer before and after acidification with 5% HCl to determine both chlorophyll *a* (Chl*a*) and pheopigment (Pheo) concentrations. The ratio Chl*a*/Pheo can be used as an indicator of algal cell degradation products due to grazing pressure (since herbivores convert chlorophyll *a* to phaeopigments) and/or cell senescence under poor growth conditions (Welschmeyer and Lorenzen 1985), Calibration was performed with pure Chl*a* standard (Parsons et al. 1984). For biogenic silica (B-SiO_2), 0.2 µm Millipore® polycarbonate filters were used and kept frozen at -80ºC. The silica on the filters was then converted to orthosilicic acid using the soda hydrolysis method (Conway et al. 1977), as modified by Paasche (1980) and determined spectrophotometrically (Ragueneau et al. 2005).

2.3.3. Phytoplankton counts

Water samples for phytoplankton community analysis were fixed in Lugol's iodine solution and cell counts were carried out using an inverted microscope following the method of Ütermöhl (1958). The organisms were counted and identified at 400x magnification, and phytoplankton

taxonomic groups were classified into i) diatoms; ii) dinoflagellates iii) cryptophytes, iv) nanoflagellates, v) prymnesiophytes, and vi) other autotrophs (which includes euglenophytes and dictyochophytes). A number of 400 individuals were systematically counted for the most abundant species. Visible cell dimensions were measured at least for five individuals for each taxon. Calculation of cell volume was obtained according to geometric forms and equations reported in Hillebrand et al. (1999).

2.3.4. Total suspended material (TSM), particulate total nitrogen (PTN) and particulate organic carbon (POC)

Samples for TSM and PTN and POC analyses were collected by filtering between 150 and 500 ml of seawater from all stations and depths using 0.7 µm pre-ashed Whatman® GF/F filters. These were kept frozen at -80ºC until analysis in the laboratory. TSM filters were freeze-dried and then weighed. PTN and POC were analyzed with a Perkin-Elmer® CHN elemental analyzer. Inorganic carbon (mainly in the form of carbonates) was removed from POC samples before analysis by repeated addition of HCl 1 N, until no effervescence was observed (Schubert and Nielsen 2000). Percentage of lithogenous inorganic particles was estimated as [(TSM-POM) x 100]/TSM, where POM=POC x 2 (Riley et al. 1970).

2.3.5. C and N bulk and stable isotopic analysis.

Prior to the δ^{13}C-POC determinations, inorganic carbon was removed from Whatman® GF/F filters using the same method as for POC described above.

Stable carbon ($^{13}C/^{12}C$) and nitrogen ($^{15}N/^{14}N$) isotopic ratios from the particulate material (δ^{13}C-POC and δ^{15}N-PTN, respectively) were determined using a FlashEA 1112 Elemental Analyzer combined with a Delta V Advantage Isotopic Ratio Mass Spectrometer (Thermo Electron Corp.,

Germany). Isotopic results were expressed relative to Vienna PeeDee Belemnite (PDB) and atmospheric nitrogen (N_2), for $\delta^{13}C$ and $\delta^{15}N$ respectively, in the conventional δ unit notation (‰) according to the following formula:

$\delta = [(R_{sample} / R_{standard}) - 1] \times 10^3$,

where $R = {}^{13}C/{}^{12}C$ for carbon and $R = {}^{15}N/{}^{14}N$ for nitrogen in the sample, and $R_{standard}$ is the value for the reference material. Precision was calculated on the basis of replicate analyses of the standards (analytical error: SD), and was · 0.1‰ for both $\delta^{13}C$ and $\delta^{15}N$.

2.3.6. Dissolved organic carbon (DOC) and chromophoric dissolved organic matter (CDOM)

DOC and CDOM samples were collected only during August and October. Collected seawater was filtered through 0.2 µm Millipore® polycarbonate filters. All glass material was previously burned (450 ºC, 4.5h). Samples for DOC were acidified with H_3PO_4 until pH 1-2, and kept in the dark at 4 °C until analysis by high temperature catalytic oxidation (HTCO) in the laboratory. DOC Consesus Reference Material (CRM: 44–45 µmol C/L^{-1} and 2 µmol C/L^{-1}) provided by D. A. Hansell and Wenhao Chen (Univ. of Miami), were used to monitor the ultimate accuracy of DOC concentration measurements. Samples for CDOM were stored at 4 ºC and kept in the dark until analysis. All samples were measured with 10 cm pathlength quartz cuvettes, using Milli-Q water as a reference on a Shimadzu dual beam UV-1800 spetrophotometer. Spectra were measured from 200 to 800 nm every 1 nm. The average absorbance value within the range 700-800 nm was subtracted from each absorbance scan to correct for scattering. Absorbance measurements were transformed to absorption coefficients (m^{-1}) by multiplying by 2.303 and dividing by the path length (0.1 m). The spectral slopes $S_{275-295}$ and $S_{350-400}$ were obtained from the regression line of the Naperian logarithms of the absorption coefficients vs. wavelengths in the range of

275-295 and 350-400 nm, respectively. These ranges were chosen because the higher variability in the slope (S) occurs in these two intervals. The S_R ratio calculated by dividing $S_{275-295}$ by $S_{350-400}$, was used as a proxy to variations in the DOM molecular weight (Helms et al., 2008). Specific ultraviolet absorbance at 254 nm ($SUVA_{254}$, L/(µgC m)) was derived dividing the absorption coefficient at 254 nm by the DOC concentration. $SUVA_{254}$ is a useful parameter for estimating the dissolved aromatic carbon content in aquatic systems (Weishaar et al. 2003).

2.3.7. Carbohydrate (CHO), Protein (PRT) and Lipid (LIP) fractions.

Colorimetric methods were used for measuring amounts of CHO, PRT and LIP within suspended materials. Total carbohydrates (CHO) were determined according to the method of Dreywood (1946), recovery by Brink et al. (1960), and expressed as glucose equivalent. Total proteins (PRT) were extracted using sodium hydroxide (NaOH 0.1 N, 2h) and concentrations (expressed in gamma globulin equivalents) were determined using the method of Bradford (1976). Total lipids (LIP) were extracted by direct elution with chloroform / methanol (2/1 v/v) and determined according to the method of Barnes and Blackstock (1973).

Biopolymeric organic carbon (BP-C) fraction was defined as the sum of carbon equivalents of total carbohydrates, proteins and lipids, using C-molar ratios of 0.4, 0.49 and 0.75, respectively (Danovaro et al. 2001).

2.3.8. Data treatment and statistical analysis

Regardless of the analysis performed all samples were collected and analyzed in triplicates for each depth/station sampled, except for the analysis of CHO, LIP and PRT where only one measurement per depth was possible. The data analysis software *JMP Statistics* was used for statistical analyses. Correlations between the investigated variables were examined with parametric

Pearson correlations. p-values below 0.05 are considered statistically significant. Table 2 shows Pearson's correlation coefficients between the variables investigated when statistical significance was met. A linear regression (model II) was performed to infer the equations from figures 6 and 7.

To summarize the vertical variability within the water column, data from each sampling station was grouped in two distinct layers: 'upper layer' which includes the averaged data from depths above and including the maximum Chl*a* fluorescence (surface and maximum Chl*a* fluorescence), and 'bottom layer' which includes the averaged data from depths below the maximum Chl*a* fluorescence (intermediate and bottom). Mean ± standard deviation values of main variables for each layer are exhibited in tables 3 and 4.

3. Results

3.1. Meteorological and hydrological conditions

Seasonal mean air temperature values (winter: -6.2 · 4.7 ºC; spring: -5.6 · 4.7 ºC; summer: 5.0 · 1.3 ºC; fall: -2.6 · 6.3 ºC) fell among model projections described in a recent study (see figure 5 from Førland et al. 2011). For comparison, we used the median value of Empirical/Statistical Downscaling (ESD) ensemble (the thick line from the mentioned figure) that predicts local climate changes in Svalbard from the output of global and regional climate models from the CMIP3 archive that used historical radiative forcings to 2000 and a range of future emissions scenarios from 2001-2100 (Meehl et al. 2007). Summer and fall mean values for 2012 were close to the median ESD value, while spring and winter mean values were both higher than it by 2.8 and 4.2 ºC, respectively. Thus 2012 appeared to be a warmer year than

predicted from future greenhouse gas and aerosol emissions, displaying particularly high winter temperatures. PAR values decreased gradually and seasonally during our sampling periods (Fig. 2B). They averaged 94 · 40 W/m^2 in May, reached its monthly maximum during June (with a mean value of 112 · 33 (SD) W/m^2), close to previous maximum irradiances recorded at Ny-Ålesund (Hanelt et al. 2001), and began to decrease in July to reach values averaging 49 · 21 W/m^2 in August, and 4 · 2 (SD) W/m^2 in October. There was a one-month time lag between PAR maximum values, recorded in June, and maximum air temperature values, recorded in July.

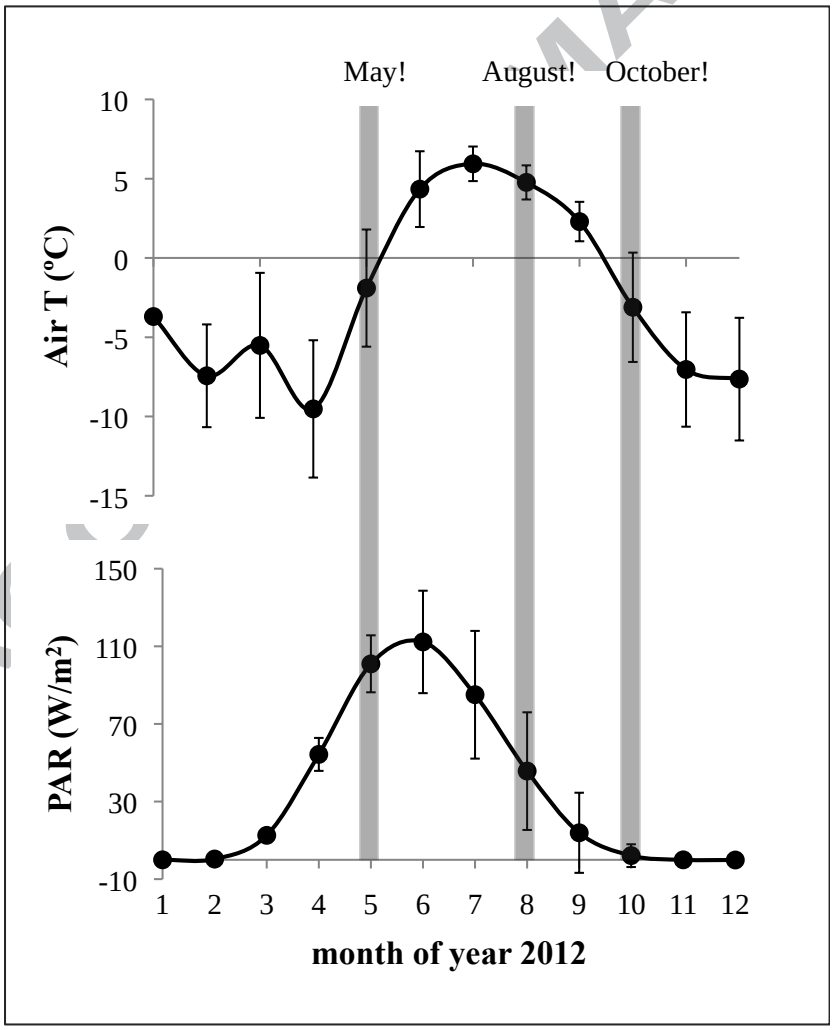

Figure 2. Monthly mean values, ± standard deviations, of Air Temperature (ºC) and the Photosynthetical Active Radiation (PAR in W/m^2) in the Kongsfjorden for 2012. Grey bars indicate the three sampling periods: Ecotab 1, during May; Ecotab 2, during August; and Ecotab 3, during October, (Data from the AWIPEV station at Ny Ålesund).

A Temperature-Salinity (T-S) diagram displaying the water masses present during the three sampling periods is shown in Figure 3. According to the definitions given by Cottier and co-workers (2005), four water masses were identified in the fjord basin: SW, IW, TAW, and AW, with characteristics summarized in Table 1. Vertical temperature, salinity, fluorescence and buoyancy frequency variability from each sampling time and station is recorded in Figure 4. Low temperature and high salinity values were observed in May, with relatively homogenous conditions across the stations and low variability in the vertical compared to other seasons (T ranging from 1.17 to 3.46 ºC and salinity ranging from 34.64 to 35.11). Late May was mainly and almost exclusively dominated by TAW with a small contribution of AW at shallow waters of the outer station (Fig. 3 and 4), indicating that AW was entering Kongsfjorden and mixing with the ArW remaining from the winter. Profiles collected in August and October indicated greater water mass variability during these seasons alongside a strengthening of stratification as indicated by the buoyancy frequency. Stronger stratification occured at shallow depths in August and at deeper depths in October (Fig. 4). The stratification at shallow waters was due to freshwater runoff from land and glaciers, creating SW that lowered the surface water salinity to

values of 31.81 at the surface of the inner station in August. Mixing between SW and underlying Atlantic water types (AW and TAW) produced IW (Fig. 3). The combination of Atlantic water inflow and local freshwater runoff also caused complex hydrographic features in August, where intrusions of warm and saline AW accentuated the temperature gradient enhancing stratification. This phenomenon can be observed in the temperature-depth profile at around 100 m in both middle and outer stations during summer (Fig. 4). In October the entire water column, at depths greater than 100 m was homogeneously dominated by AW as revealed by temperatures higher than 3ºC prevailing in the water column below 20 m (Fig. 3). SW and IW were also present at shallower depths (upper 20 m), although they showed higher salinity and cooler temperature than those observed during August. In general, the water column appeared to be more stratified in summer and fall compare to the spring as indicated by high values of the buoyancy frequency (Fig 4.). One observes a stratification gradient that decrease with the distance from station A to station B as the influence of fresh water decrease for all seasons.

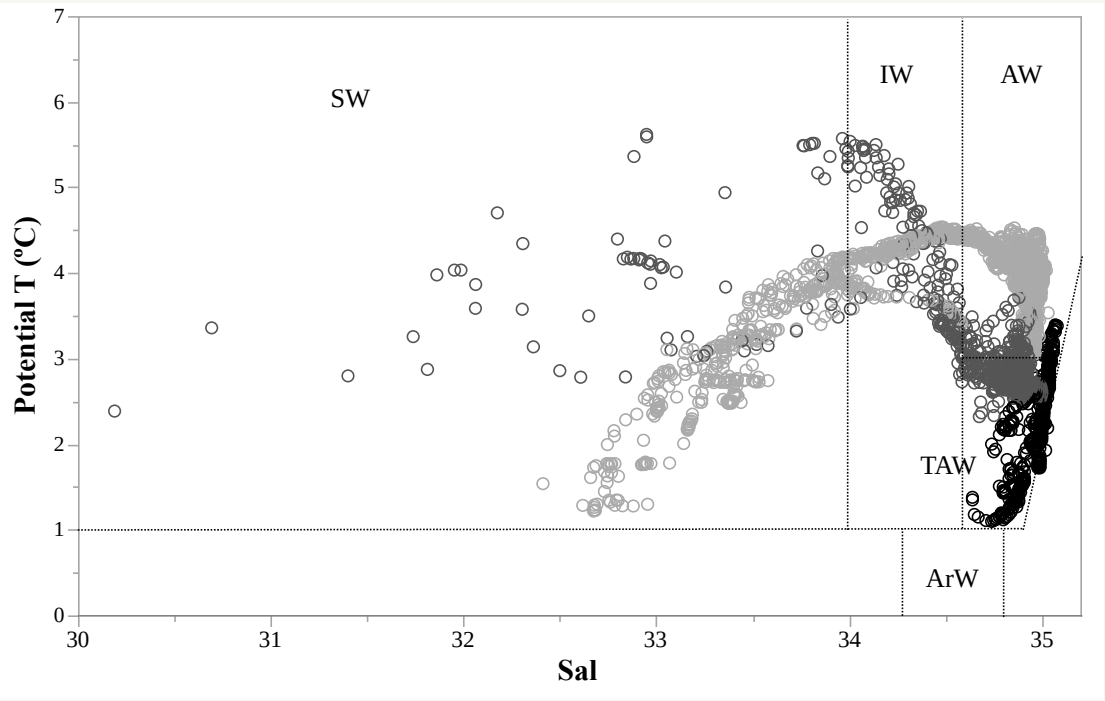

Figure 3. T-S diagram of vertical CTD profile data obtained in 2012 at Inner, Middle and Outer stations during May (black circles), August (dark grey circles) and October (clear grey circles). The data are superimposed on the water mass domains described in the Introduction; Arctic Water (ArW); Transformed Atlantic Water (TAW), Atlantic Water (AW); Intermediate Water (IW); and Surface Water (SW).

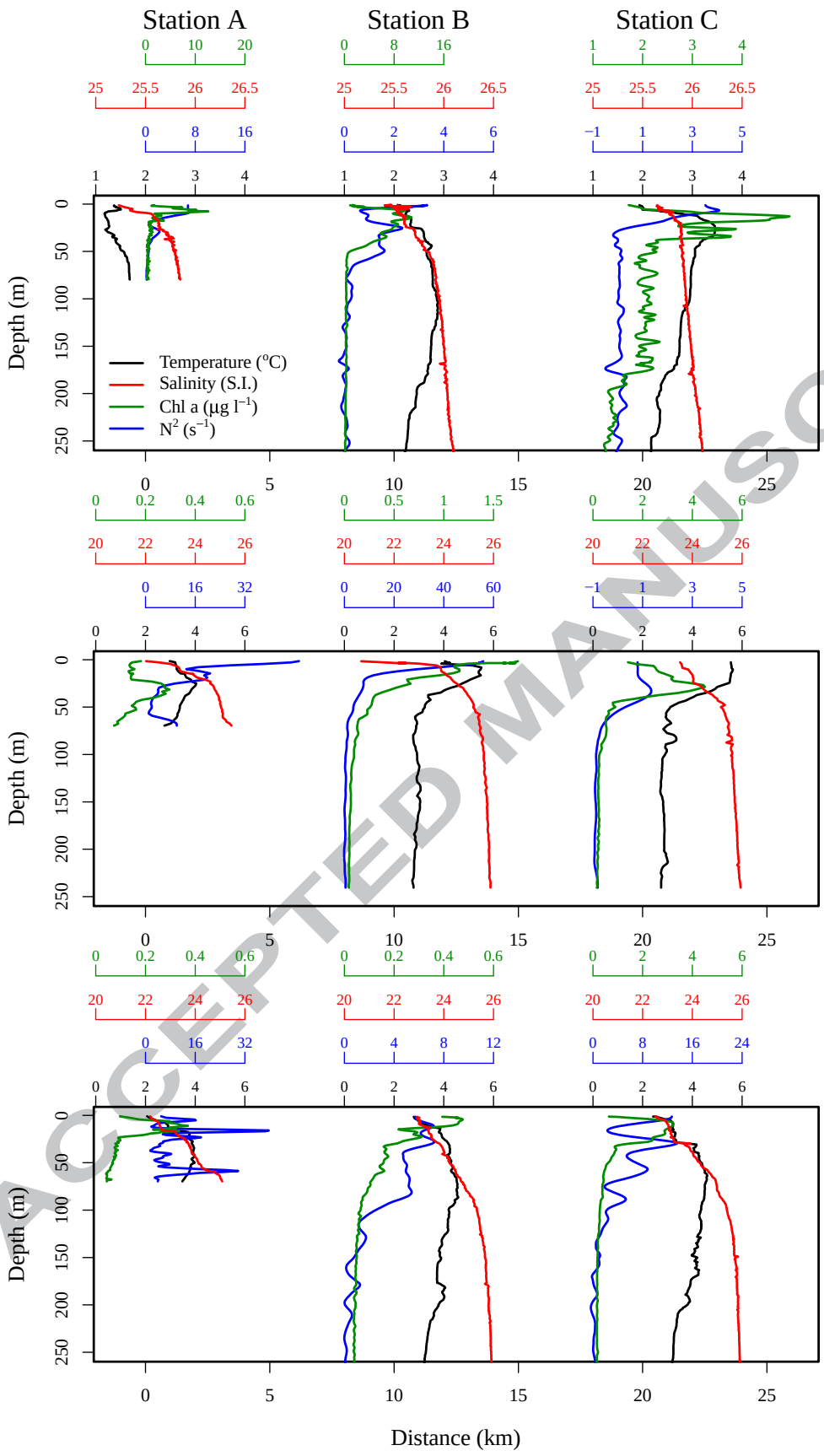

Figure 4. Vertical profiles of Temperature (T, ºC, black), Salinity (Sal, S.I., red), Chlorophyl a (Chla, µg/L, green) and buoyancy frequency (N^2, s^{-1}, blue) during May (upper panel), August (central panel) and October (lower panel) at the three stations sampled. X-axis represents the distance to the fjord head so that data from station A (inner-fjord, 80 m depth), station B (mid-fjord, 350 m water depth) and station C (outer-fjord, 300m depth) are displayed at the left, mid and right panels respectively. Note change of scale between panels.

3.2. Nutrients

All nutrients showed a variable distribution throughout the upper and lower water column in the fjord (Table 3; see Table 1 and Figures 1 and 2 in Supplementary Material for additional detail). Concentrations, in µmol/L, ranged between 0.37 and 10.81 for NO_3^-, 0.03 and 0.36 for NO_2^-, 0.12 and 2.86 for NH_4^+, 0.18 and 4.50 for $Si(OH)_4$, and 0.05 and 0.66 for PO_4^{3-}. Highest concentrations of nitrate, silicate and phosphate were measured in May and minima were measured in August. Reduced inorganic nitrogen (nitrite and ammonia) followed different concentration patterns: highest concentrations of nitrite were found in October, and minimum concentrations in May, while ammonia exhibited highest concentrations in August and the lowest in May (Table 3), opposite to seasonal patterns of nitrate, silicate and phosphate. Ammonia significantly and linearly decreased with higher salinities (R^2=0.16, P<0.05, Table 2), particularly for salinity values lower than 34.5, corresponding to SW and IW masses (R^2=0.35, n= 14, P<0.05). The linear correlation was lost for salinities higher than 34.5, corresponding to AW and TAW masses. During the May spring bloom, all nutrients (except ammonia) linearly and significantly decreased when Chl*a* concentration increased (NO_3^-, R^2= 0.76; NO_2^-, R^2=0.56;

$Si(OH)_4$, R^2=0.65; PO_4^{3-}, R^2=0.71, P <0.05 for all the relationships, Table 2). All nutrients consistently increased with depth independently of the location within the fjord and the season sampled, except for ammonia, which showed a significant decrease with depth during October. Interestingly, nitrite also showed a strong decrease with depth in October. Si:N ratios, calculated considering N as the sum of all dissolved inorganic nitrogen (DIN= $[NO_3^-]$ + $[NO_2^-]$ + $[NH^{4+}]$), statistically and significantly increased when salinity decreased (R^2=0.55, P<0.001, Table 2).

Spatial variability in nutrient concentrations was lower than seasonal variability. However, the outer fjord displayed higher nutrient concentrations than the inner and middle fjord, in both upper and bottom layers, during the May spring bloom. A similar pattern was observed during August and October but only with nitrate and phosphate at the bottom water layer. On the contrary, ammonia and nitrite concentrations at the bottom layer decreased towards the outer fjord during fall.

		Chl*a* µg/L	B-SiO_2 µg/L	Sal *S.I.*	T ºC	NO_3^- µmol/L	$\delta^{13}C$ ‰	C:N	Diatom Ab cell/L	cryptophytes %
NO_3^-	µmol/L	0.76* M								
NO_2^-	µmol/L	0.56* M								
NH_4^+	µmol/L			0.16* ALL						
PO_4^{3-}	µmol/L	0.71* M								
$Si(OH)_4$	µmol/L	0.65* M	0.80** M							
Diatom Ab	cell/L	0.88*** ALL	0.79*** ALL							
Si:N				0.55*** ALL						
cell size	µm³				0.23* ALL					
TSM	mg/L									
POC	mg/L	0.78** M								
		0.36** A&O								
$\delta^{13}C$	‰	0.68** M		0.44** A&O						
$\delta^{15}N$	‰					0.62* M	0.50* M			
$SUVA_{254}$	L/(µgC m)			0.33* ALL			0.37* ALL			
$S_{350-400}$	μm^{-1}			0.35* ALL						
S_R	μm^{-1}			0.39* ALL						
BP-C	%							0.30** ALL		
PRT	µg/L								0.75** ALL	
LIP	%									0.18* ALL

Table 2. Pearson's correlation coefficients between the variables investigated when statistically significant (P<0.05). Abbrebiated terms are Chlorophyll *a* (Chl*a*), Biogenic Silica (B-SiO_2),

Salinity (Sal), Temperature (T), nitrate (NO_3^-), Carbon isotopic ratio ($\delta^{13}C$), Carbon to Nitrogen molar ratio (C:N), diatom abundance (Diatom Ab), nitrite (NO_2^-), ammonia (NH_4^+), phosphate (PO_4^{3-}), silicate ($Si(OH)_4$), Silica to Nitrogen molar ratio (Si:N), total suspended material (TSM), particulate organic carbon (POC), Nitrogen isotopic ratio ($\delta^{15}N$), specific UV absorbance at 254 nm ($SUVA_{254}$), Spectral slope between 350-400nm ($S_{350-400}$), Spectral slope ratio (S_R), Bio-polymeric Carbon (BP-C), Proteins (PRT) and Lipids (LIP). * indicates correlations where $P<0.05$, ** indicates correlations where $P<0.01$ and *** indicates correlations where $P<0.001$. ^{M} indicates correlations with data from May, $^{A\&O}$ indicates correlations with data from August and October and ^{ALL} indicates correlations with all data.

3.3. Fluorescence, Chla and pheopigments

CTD data recorded the highest fluorescence peak (>10 µg/L) during late spring (May) in the surface layer of inner (7 m depth) and middle fjord (25 m depth) stations, reaching values 1.5 orders of magnitude higher than the maximum Chl*a* fluorescence peaks recorded during August and October (< 1µg/L) (Fig. 4). In agreement with the fluorescence probe, a massive maximum Chl*a* biomass peak was analytically measured during the phytoplankton bloom in May, with concentrations reaching values up to 15.5 µg/L in the upper layers of the inner station (Table 3). In August and October Chl*a* maximum concentration measured in the inner fjord upper layer drastically decreased to 0.2 µg/L, which corroborates the fluorescence data. Averaged Chl*a*:Pheo ratios from the upper layer were about 7, 4 and 2 times higher during May than August and October values, for inner, middle and outer fjord stations, respectively (Table 3). These spatial and temporal shifts reflect mainly the high contents of Chl*a* in surface waters of the inner and middle stations in May. The lower ratios (<1), particularly at depths higher than 200 m at the

outer and middle stations during August and October, indicate higher contributions of pheopigments related to Chl*a*.

	Station		Chl*a*	Chl*a*/Pheo	NO_3^-	NO_2^-	NH_4^+	PO_4^{3-}	$Si(OH)_4$	B-SiO_2	Total Abundance
			µg/L		µmol/L	µmol/L	µmol/L	µmol/L	µmol/L	µg/L	cell/L
May	Inner	upper	15.53	9.81	1.00	0.05	0.12	0.14	0.45	2.72	$1.7\ 10^6 \pm 8.5\ 10^5$
		bottom	2.67 ± 2.15	5.36 ± 2.26	9.05 ± 1.48	0.16 ± 0.03	0.68 ± 0.23	0.54 ± 0.12	2.80 ± 0.80	0.69 ± 0.57	$3.0\ 10^5 \pm 1.4\ 10^5$
May	Middle	upper	12.08	5.55	0.37	0.03	0.16	0.05	0.18	2.22	$1.2\ 10^6 \pm 2.3\ 10^5$
		bottom	1.68 ± 2.3	2.15 ± 2.7	7.20 ± 4.7	0.10 ± 0	0.88 ± 0.1	0.48 ± 0.3	2.54 ± 2.7	0.64 ± 0.7	$6.3\ 10^4 \pm 7.5\ 10^4$
May	Outer	upper	2.32	2.63	4.81	0.07 ±	1.90	0.33	1.83	0.76	$4.3\ 10^5 \pm 1.3\ 10^5$
		bottom	0.35 ± 0.4	0.89 ± 0.9	10.81 ± 0.2	0.15 ± 0	0.75 ± 0.6	0.66 ± 0	3.96 ± 0.3	0.13 ± 0.2	$1.9\ 10^4 \pm 2.2\ 10^4$
Aug	Inner	upper	0.22 ± 0.11	1.24 ± 1.36	1.96 ± 2.13	0.17 ± 0.07	2.50 ± 0.55	0.16 ± 0.06	2.54 ± 2.03	0.05 ± 0.07	0.0
		bottom	0.11	0.57	1.02	0.20	2.86	0.27	1.28	0.59	$2.0\ 10^3$
Aug	Middle	upper	0.36 ± 0.10	1.31 ± 0.46	0.54 ± 0.33	0.10 ± 0.03	1.71 ± 0.29	0.15 ± 0.03	1.53 ± 0.49	0.06 ± 0.05	$3.9\ 10^4$
		bottom	0.04 ± 0	0.09 ± 0.1	4.31 ± 4	0.31 ± 0.3	2.57 ± 0.24	0.51 ± 0.3	4.50	0.22	$1.6\ 10^4$
Aug	Outer	upper	0.52 ± 0.18	1.13 ± 0.06	0.88	0.05	0.93	0.11	0.72	0.15	$5.6\ 10^4$
		bottom	0.07 ± 0.1	0.19 ± 0.2	6.13 ± 5.3	0.30 ± 0.2	2.27 ± 0.13	0.51 ± 0.3	2.67 ± 1.9	0.19 ± 0	$1.1\ 10^4$
Oct	Inner	upper	0.24 ± 0.01	1.50 ± 0.28	2.18 ± 0.04	0.28 ± 0.06	1.70 ± 0.28	0.25 ± 0.01	1.95 ± 0.01	0.05	$3.5\ 10^4$
		bottom	0.04	0.44	2.29	0.22	1.76	0.30	1.66	0.08	$6.2\ 10^3$
Oct	Middle	upper	0.31 ± 0.03	1.28 ± 0.19	1.53 ± 0.06	0.36 ± 0.25	1.62 ± 0.08	0.31 ± 0.11	1.61 ± 0.01	0.00	$8.8\ 10^4$
		bottom	0.04 ± 0	0.23 ± 0	6.87 ± 4.2	0.15 ± 0.2	0.56 ± 0.5	0.52 ± 0.2	3.23 ± 1.6	0.03 ± 0	$3.6\ 10^4$
Oct	Outer	upper	0.48 ± 0.02	1.31 ± 0.06	1.28 ± 0.45	0.17 ± 0.06	1.61 ± 0.47	0.39 ± 0.19	1.55 ± 0.34	0.10 ± 0.01	$4.7\ 10^5$
		bottom	0.05 ± 0.1	0.34 ± 0.1	5.86 ± 5.7	0.11 ± 0.1	0.84 ± 1.1	0.48 ± 0.3	2.88 ± 2.1	0.37 ± 0.1	$4.1\ 10^3$

Table 3. Mean ± standard deviation values measured, at the upper and bottom water layers, for Chlorophyll *a* (Chl*a*, µg/L), Chlorophyll *a* / Pheopigments (Chl*a*/Pheo), nitrate (NO_3^-, µmol/L), nitrite (NO_2^-, µmol/L), ammonia (NH_4^+, µmol/L), phosphate (PO_4^{3-}, µmol/L), silicate ($Si(OH)_4$, µmol/L), Biogenic Silica (B-SiO_2, µg/L), total phytoplankton cell abundance (cell/L), within each station (Inner, Middle and Outer fjord) and for each sampling period (May, August and October).

3.4. Phytoplankton abundance, composition and distribution.

There was a pronounced difference in phytoplankton community between May, August and October (Table 3 and Fig. 5). Maximum cell numbers (1.7×10^6 cells/L) were encountered in May, at the upper layer of the inner fjord, coincident with the maximum peak of Chl*a*. During

the bloom the values decreased gradually towards the open edge of the fjord, and exponentially with depth, with minimum values found at the bottom of the outer station (1.9×10^4 cells/L). On a seasonal scale, cell counts decreased drastically in August (about six orders of magnitude for the upper layer of the inner most station, and two orders of magnitude for middle and outer stations), and increased again slightly in October (Table 3). Contrasting to late spring, higher abundances were found in the upper layer of the outer fjord during summer and fall (5.6×10^4 cells/L and 4.7×10^5 cells/L respectively).

The algal major groups also changed markedly between seasons and stations. In May, diatoms represented more than 80% of the main phytoplankton groups at all stations, completely dominating (> 98%) at the inner fjord (Fig. 5). They disappeared almost completely in summer and autumn, causing a drop in biomass. Accordingly biogenic silica ($B\text{-}SiO_2$) drastically decreased in the upper 50 m from spring through summer and fall (Table 3). Diatom abundance was positively correlated with Chl*a* and $B\text{-}SiO_2$ values ($R^2 = 0.88$ and $R^2 = 0.79$ respectively, $P<0.001$, Table 2) and $B\text{-}SiO_2$ significantly increased with a decrease in inorganic silicate during the bloom ($R^2 = 0.80$, $P < 0.01$, Table 2). August was characterized by very low cell numbers especially at the inner fjord. The slight increase in phytoplankton cells during October consisted mainly of nanoflagellates, dominating the inner fjord, and of cryptophytes and dinoflagellates dominating the outer fjord (Fig. 5). The dominance of prymnesiophytes during August in ST A is somehow over-represented in figure 5, as it corresponds to only a few number of cells (see Table 3). Cell size (μm^3) significantly decreased with increasing temperature ($R^2= 0.23$, $P<0.02$, Table 2).

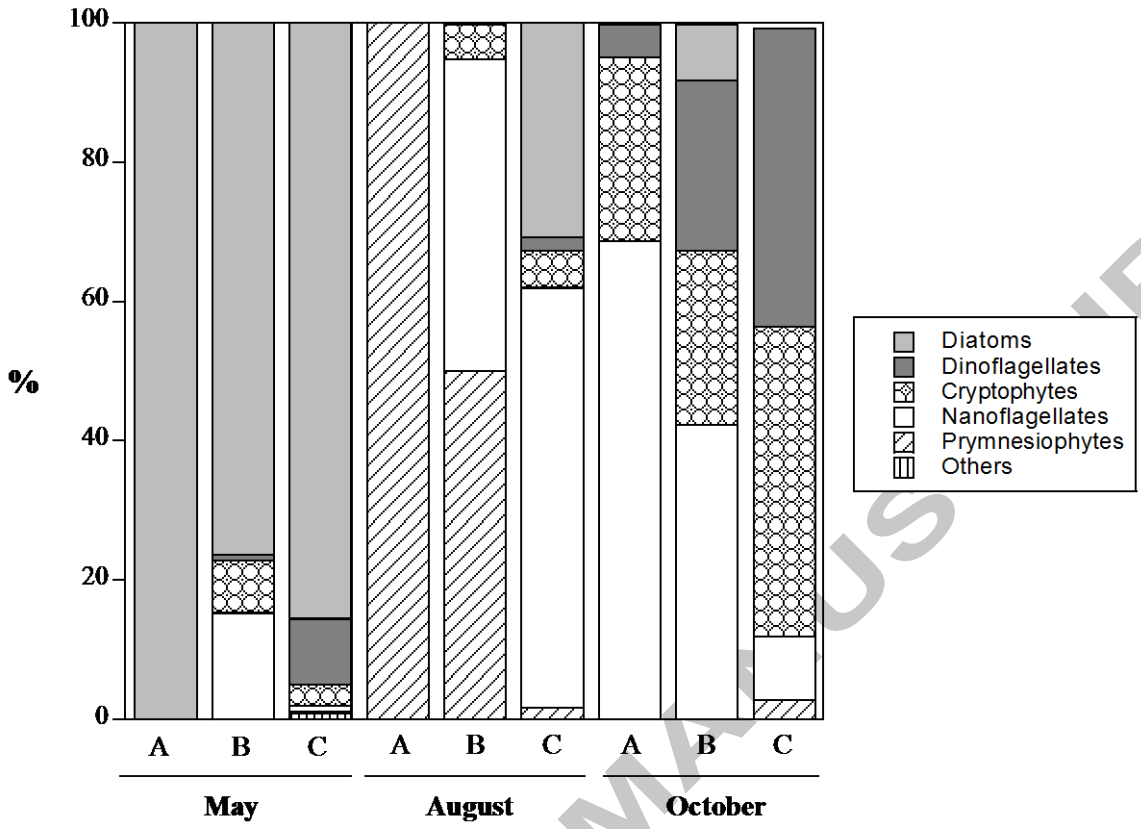

Figure 5. Relative contributions (%) of diatoms, dinoflagellates, cryptophytes, nanoflagellates, prymnesiophytes and other cells to the total abundance of cells (cell/L) in the 3 stations sampled (A: inner-fjord; B: mid-fjord; C: outer-fjord) at the three different seasons in 2012. Data have been averaged per station.

3.5. TSM and POC: elemental, isotopic and biochemical composition.

Total suspended material (TSM) showed, on average, higher concentrations in the inner fjord (6.4 ± 3.1 mg/L) than in the middle and outer fjord (4.4 ± 3.0 and 2.6 ± 2.9 mg/L, respectively) (Table 4). TSM significantly and linearly decreased with salinity for salinity values lower than 34.5, corresponding to SW and IW masses (R^2=0.53, n= 14, P<0.05). The linear correlation was

lost for salinities higher than 34.5, corresponding to AW and TAW masses. On a seasonal basis, loads were higher in May (ranging from 12.1 to 3.6 mg/L) and decreased to 9.0 - 0.5 and 4.6 – 1.0 mg/L in August and October, respectively. TSM values were generally higher in the upper than in the bottom layers, but in October vertical differences became smaller (Table 4). Particulate organic carbon and nitrogen contents (POC, PTN in mg/L) followed the same seasonal pattern as TSM with higher averaged values in May (0.24 ± 0.19 mg/L for POC and 0.04 ± 0.03 mg/L for PTN) than in August (0.13 ± 0.06 mg/L for POC and 0.02 ± 0.01 mg/L for PTN) and October (0.08 ± 0.03 for POC and 0.02 ± 0.01 for PTN) (Fig. 6). However, their relative content to TSM (POC-% and PTN-%) was lower than 11% and 3%, respectively, and exhibited a complex pattern with time and space (Table 4). The outer station was characterized by POC and PTN-rich material, displaying values of POC > 9 % and of PTN > 1% in the upper layer during both August and October periods (Table 4). On the contrary, the inner fjord showed relatively high POC percentage values during May (3.01-4.48 %) which decreased in August and remained low in October (around 1.6 %). There was a strong relationship between POC (mg/L) and Chl*a* (µg/L), during the spring bloom (R^2=0.78, P=0.002, Table 2). This relationship weakened during August and October (R^2= 0.36, P<0.01, Table 2).

POC and $\delta\,^{13}$C-POC values were higher in May and seasonally decreased during August and October. $\delta\,^{13}$C displayed high variability in May, ranging from -27.7 to -22.7 ‰. ^{13}C depleted values were the norm during summer and fall (averaging -26.5 ±0.7). Seasonal variations were larger than spatial variations for the inner and middle stations (Table 4).

Station			TSM	POC	PTN	C:N	$\delta^{13}C$	$\delta^{15}N$	CHO	LIP	PRO	BP-C
			mg/L	%	%		‰	‰	µg/L	µg/L	µg/L	%
May	Inner	upper	12.1	4.48	0.75	7.01	-23.2	1.9	84.9	84.1	148.3	31.4
		bottom	4.4 ± 0.8	3.01 ± 0.58	0.53 ± 0.17	6.82 ± 0.88	-24.7 ± 0.8	-0.5 ± 1.5	78.9 ± 94.8	4.7 ± 6.7	0.4	
May	Middle	upper	9.6	6.80	0.95	8.32	-22.7	1.4	293.2	166.9	120.4	46.3
		bottom	6.1 ± 2.8	3.46 ± 3	0.41 ± 0.4	10.22 ± 0.8	-25.4 ± 1.7	-0.5 ± 5.3	73.9 ± 49.4	68.2 ± 5.6	19.5 ± 27.6	35.7
May	Outer	upper	8.2	4.53	0.79	6.72	-25.8	1.9	43.5	79.4	64.9	29.2
		bottom	3.6 ± 0.8	4.60 ± 2.7	0.96 ± 0.7	5.99 ± 1.1	-27.7 ± 0.1	-3.0 ± 1.3	167.4	31.2 ± 30.6	57.2	52.1
Aug	Inner	upper	9.0 ± 0.9	1.53 ± 0.03	0.27 ± 0.01	6.72 ± 0.09	-26.7 ± 0.7	0.2 ± 0.5	10.6 ± 0.0	28.1 ± 10.5	16.0 ± 1.5	24.5 ± 8.1
		bottom	6.1	1.69	0.28	6.96	-26.0	1.1	16.1	26.0	8.5	29.2
Aug	Middle	upper	5.3	2.39	0.54	5.03 ± 0.20	-27.1 ± 1.8	1.4 ± 2.7	11.5 ± 6.4	29.7 ± 12.3	34.6 ± 3.9	41.3 ± 20.0
		bottom	0.5	10.50	2.14	7.53 ± 2.6	-25.6 ± 1.1	0.9 ± 2.5	7.6	14.9	6.0	33.8
Aug	Outer	upper	2.0 ± 0.5	10.88 ± 1.43	1.18 ± 0.22	10.82 ± 0.60	-27.1 ± 0.3	2.4 ± 1.0	19.3 ± 2.6	20.7 ± 0.8	31.5 ± 6.0	17.7 ± 0.4
		bottom	1.8 ± 0.3	5.29 ± 1.2	0.75 ± 0	8.20 ± 1.5	-25.8 ± 2.3	-0.5 ± 1.5	7.3 1.2	12.0 ± 7.5	7.5 ± 1.4	16.7 ± 8.6
Oct	Inner	upper	4.6 ± 1.2	1.79 ± 0.23	0.56 ± 0.05	3.76 ± 0.80	-26.3 ± 0.5	0.5 ± 1.0	1.6	92.0	12.1	84.8
		bottom	3.1	1.54	0.76	2.36	-26.6	1.5	10.9	28.1	5.6	59.4
Oct	Middle	upper	2.1 ± 0.5	5.02 ± 1.08	0.43 ± 0.27	15.99 ± 7.09	-26.3 ± 0.0	2.1 ± 0.7	2.5	45.4	5.9	36.3
		bottom	3.6 ± 2.3	2.52 ± 2.4	0.28 ± 0.2	10.12 ± 1.3	-26.6 ± 0.6	-0.4 ± 0.3	5.5 ± 1.7	16.7 ± 7.6	4.8 ± 1.8	31.0 ± 19.9
Oct	Outer	upper	1.0 ± 0.1	9.94 ± 0.58	1.47 ± 0.41	8.27 ± 2.75	-27.1 ± 0.2	0.1 ± 1.1	11.6	19.2	25.8	32.5
		bottom	1.5 ± 0.3	5.56 ± 2	1.26 ± 1	6.26 ± 2.9	-26.4 ± 0.7	-0.2 ± 1.0	8.4 ± 2.5	11.7 ± 2.2	5.6 ± 3.9	18.1 ± 4.6

Table 4. Mean ± standard deviation values measured, at the upper and bottom water layers, for Total Suspended Material (TSM, mg/L), Particulate Organic Carbon fraction (POC, %), Particulate Total Nitrogen fraction (PTN, %), Carbon ($\delta^{13}C$, ‰) and Nitrogen ($\delta^{15}N$, ‰) isotopic ratios of POC and PTN respectively, contents in Carbohydrates (CHO, µg/L), Lipids (LIP, µg/L), Proteins (PRT, µg/L), and total of the Bio-polymeric Carbon fraction, within each station (Inner, Middle and Outer fjord) and for each sampling period (May, August and October).

During the spring bloom in May, $\delta^{13}C$ linearly and significantly correlated with Chl*a* (R^2=0.68, n=9, P<0.01, Figure 6, Table 2), with higher $\delta^{13}C$ in the upper layers of the inner and middle stations (-23.2 and -22.7 ‰, respectively). During August and October, $\delta^{13}C$ values strongly and significantly correlated with salinity (R^2=0.44, n=21, P<0.01, Table 2), identifying $\delta^{13}C$ depleted material at lower salinities. This correlation gets stronger when only August values are considered (R^2=0.68, n=10, P<0.01). Means of nitrogen stable isotope ratios ($\delta^{15}N$) of PTN varied between -3.0 ‰ and 2.4 ‰. During the bloom in May $\delta^{15}N$ significantly decreased with increasing concentrations of nitrate (R^2=0.62, n=9, P<0.05, Table 2) and increased with

increasing values of $\delta^{13}C$ (R^2=0.50, n=9, P<0.05, Table 2) (Fig. 7). $\delta^{15}N$ showed little variation during summer and fall and displayed consistently low values, averaging 0.7 ‰ (± 1.4 SD).

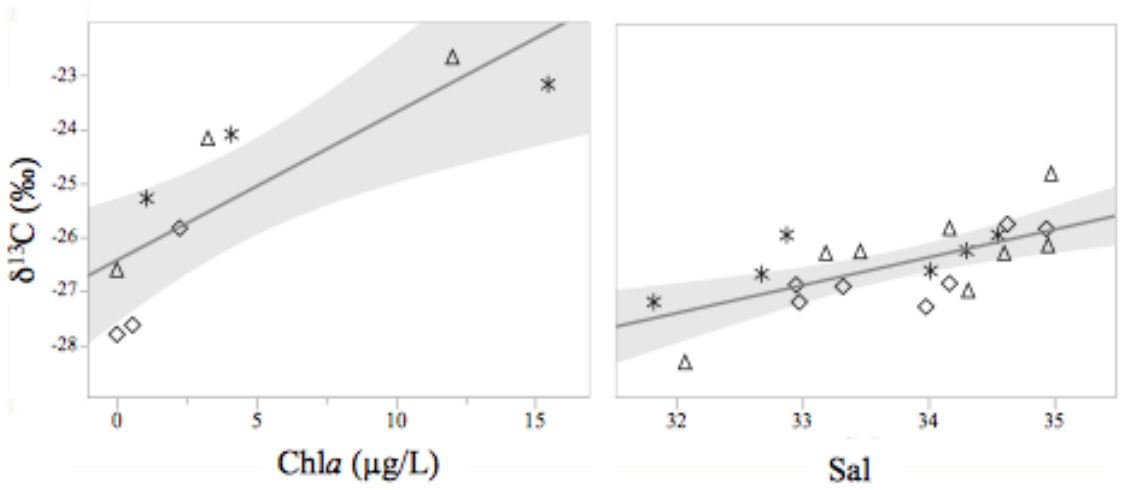

Figure 6. Relationship between $\delta^{13}C$ ratio (‰) and Chl*a* (µg/L) during May, (left panel), and relationship between $\delta^{13}C$ ratio (‰) and salinity during August and October (right panel). Stars, triangles and diamonds correspond to data from inner (ST A), middle (ST B) and outer (ST C) fjord stations, respectively. The solid line in the left panel represents the fitted linear equation $\delta^{13}C$ (‰) = -26.5 (± 0.5) + 0.3 (± 0.1) Chl*a* (µg/L), (R^2 = 0.68, P < 0.01), while the solid line in the right panel from represents the fitted linear equation $\delta^{13}C$ (‰) = -44.0 (± 4.5) + 0.5 (± 0.1) Sal, (R^2 = 0.44, P < 0.01). The shaded area in both panels represents the confidence interval for each linear fit.

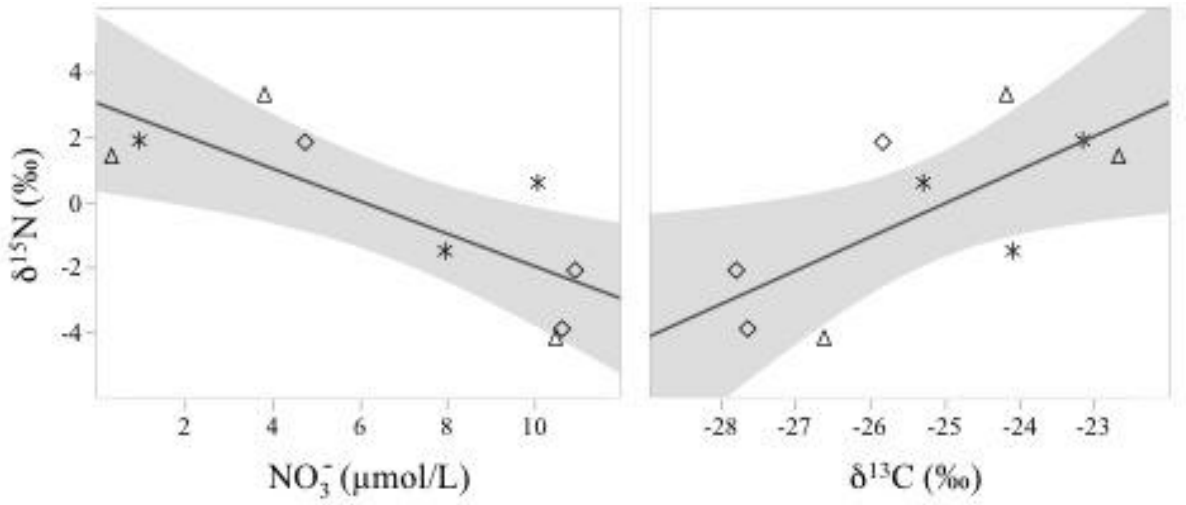

Figure 7. Relationship between $\delta^{13}N$ ratio (‰) and nitrate concentration (NO_3^-, µmol/L) (left panel), and relationship between $\delta^{15}N$ ratio (‰) and $\delta^{13}C$ (‰), during the bloom in May. Stars, triangles and diamonds correspond to data from inner (ST A), middle (ST B) and outer (ST C) fjord stations, respectively. The solid line in the left panel represents the fitted lineal equation $\delta^{15}N$ (‰) = 3.1 (± 1.2) - 0.5 (± 0.1) NO_3^- (µmol/L) (R^2 = 0.62, P < 0.05) 0.62, P < 0.01). The solid line in the right panel represents the fitted lineal equation $\delta^{13}N$ (‰) = 25.7 (± 9.8) + 1.0 (± 0.4) $\delta^{13}C$ (‰) (R^2 = 0.50, P < 0.05). The shaded area in both panels represents the confidence interval for each linear fit.

For a detailed biochemical analysis of POC, the Biopolymeric carbon (BP-C) fraction together with carbohydrate (CHO), lipid (LIP) and protein (PRT) concentrations are listed in Table 4. Biopolymeric carbon fraction (BP-C/POC (%)) varied between 16.7 and 84.8 %, with the highest variability observed during October (Table 4). It accounted, on average, for 33 % of total POC, and was significantly negatively correlated with C:N molar ratios (R^2= 0.30, P<0.01, Table 2). The fraction of BP-C in the upper layer of the inner fjord changed from 31.4 and 24.5 % in spring and summer, respectively, to 84.8 % in the fall. Summer exhibited the lowest percentages of BP-C except for the upper layer of the middle station. The seasonal means of the

carbohydrates and proteins showed higher concentrations (up to 293 µg/L for CHO and 148 µg/L for PRT) during the spring bloom than in summer and fall (< 20 µg/L for CHO and < 35 for PRT). LIP and PRT were always more abundant in the upper layers of each station. Contrastingly CHO showed higher concentrations in the bottom layer of the inner fjord during August and October (Table 4). Changes in the relative contribution of each biochemical class are represented in Figure 8. CHO, PRT and LIP have a similar contribution in spring, while CHO and PRT % tend to decrease seasonally thus increasing the % of LIP within the BP-C carbon during August and October (Figure 8). Changes in PRT content was significantly positively correlated with diatom cells abundance (R^2= 0.75, P<0.01, Table 2). Changes in the percentage of LIP was significantly positively correlated with the relative abundance of cryptophytes (R^2= 0.18, P<0.05, Table 2).

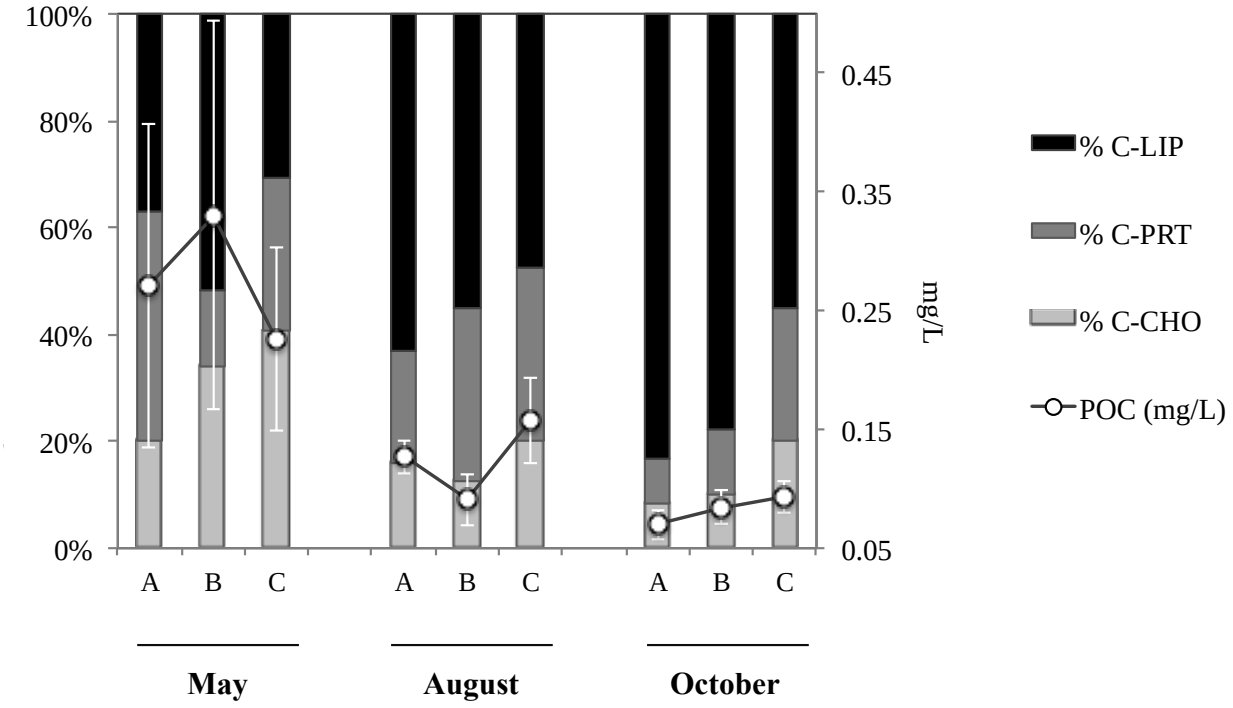

Figure 8. Relative contributions (%) of C-Lipids (C-LIP), C-Proteins (C-PRT) and C-Carbohydrates (C-CHO) to the biopolymeric carbon, and the corresponding particulate organic carbon (POC, in mg/L) in the 3 stations sampled (A: inner-fjord; B: mid-fjord; C: outer-fjord) during the three different seasons in 2012. Data have been averaged per station. Error bars correspond to the standard error (SE) of the averaged total BP-C.

3.6. Absorbance spectral slopes and $SUVA_{254}$ values.

Absorbance measurements and its derived spectral slopes were obtained only during August and October. $S_{275-295}$ varied between 28.5 and 33.8 μm^{-1} (average 30.5 · 1.4 μm^{-1}), while $S_{350-400}$ values ranged between 13.1 and 19.3 μm^{-1} (average 15.8 · 1.5 μm^{-1}). Both $S_{275-295}$ and $S_{350-400}$ showed higher values during the summer. Changes in S_R were mainly driven by changes in $S_{350-400}$, and varied between 1.6 and 2.2, with the lowest values in August. $S_{350-400}$ and S_R displayed a significant relationship with salinity, with $S_{350-400}$ decreasing and S_R increasing with increasing salinities (R^2=0.35, P<0.05 and R^2=0.39, P<0.05, respectively, Table 2). $SUVA_{254}$, is routinely used to assess dissolved organic matter sources in aquatic ecosystems and is often related to the percentage of aromatic compounds (Stubbins et al 2008, Spencer et al. 2014), was significantly negatively correlated with salinity and δ^{13}C-POC values (R^2=0.33, P<0.05 and R^2=0.37, P<0.05, respectively, Table 2).

4. Discussion

4.1. Phytoplankton and nutrient dynamics related to hydrological conditions

The mid-May phytoplankton bloom had record high concentration of cells at the upper waters of the fjord inner-most station that was under the influence of glacial meltwater, as evidenced by the low surface salinities (< 34.7) (Fig. 3 and Fig. 4) and substantial TSM discharge (Table 4). The water, not yet stratified, was clear enough so that light availability in the water column allowed phytoplankton to grow. Our results captured the bloom between the 18 and 21 of May 2012, consistent with observations from 2010, under a mixed water column dominated by the TAW (Fig. 2 and 3). The bloom occurred when the incoming light was reaching its annual maximum, air T was increasing at its highest rate (0.3 ºC per day, Fig 2) and sea surface T averaged 1.9 · 0.5 ºC, similar to SST reported in the fjord by mid May 2010 when a strong bloom (Chl*a* ~ 10 µg/L) was also detected (Kubiszyn et al. 2014). The bloom we observed was the strongest one ever reported in Kongsfjorden, peaking at 15.5 µg Chl*a*/L and comparable to the particularly dense bloom of 2006 (13 µg Chl*a*/L, Hegseth and Tverberg 2013). Likewise observed nitrate concentrations exceeded those reported elsewhere for Kongsfjorden (e.g. Hodal et al. 2012; Hegseth and Tverberg 2013).

Shifts in the timing of the bloom in Kongsfjorden between mid April and the end of May have been attributed to variability in sea ice cover and inflow of warm AW. Historically, when the fjord was covered by ice in winter, the bloom used to take place in mid-late May when sea ice started to melt (Eilertsen et al. 1989, Wictor et al 1999). Increased warming has left the fjord mostly ice-free during the period from 2007-2016 with several studies predicting a shift to earlier blooms (i.e. mid/late April) as observed in 2002, 2006 and 2008 (Hegseth and Tverberg 2008, Iversen and Seuthe 2011, Hodal et al 2012, Piquet et al. 2014). However, blooms have also been documented during mid/late May for 2003, 2004, 2007, 2010, 2012 and 2014 (Leu et al. 2006,

Hegseth and Tverberg 2008, Kubiszyn et al. 2014, Van De Poll 2016, this study), and even during late June for 2009 (Kubiszyn et al. 2014), making it difficult to identify a common bloom timing under ice free conditions. The start of glacial melt water, likely driven by the increase of both the air temperature and the heat from AW intrusion, may be shaping the time and location of the bloom, as recently suggested (Van De Poll 2016). The intensity of the bloom in Kongsfjorden has also shown high inter-annual variability ranging from very weak blooms with Chl*a* maximum peaks as low as 2µg/L in 2008 and 2009 (Kubiszyn et al. 2014; Piquet et al. 2014), to strong dense blooms with Chl*a* peaking 13µg/L in 2006 (Hegseth and Tverberg 2013). High variability in bloom timing over the last decade highlights the large uncertainties surrounding the underlying forcing impacting bloom initiation and intensity in Kongsjorden.

During May, the significant decrease of nitrate, phosphate and silicate with increasing Chl*a* provides evidence for the consumption of nutrients during the phytoplankton growth, with N:P ratios (NO_3^-:PO_4^{3-} balance) close to Redfield ratios (14 · · ·) and thus coupled to the phytoplankton metabolic requirements. We observed a high seasonal variability of nitrate values, in the bottom layer of the inner fjord, concurrent with changes in ammonia. High nitrate and low ammonia concentrations were observed during the spring bloom (9 µM and 0.7 µM, respectively at the bottom layer of the inner station), whereas those concentrations dropped down to 1-2 µM for nitrate and build up to 2-3 µM for ammonia in August and October. We hypothesize that the nitrate excess during the bloom could be due to the microbial nitrification of glacial ammonium runoff, as it has been previously suggested for high nitrate concentrations in glacial meltwaters in Kongsfjorden (Wynn et al. 2007). During August and October glacier meltwater input increased, leading to accumulation of ammonia and low nitrate concentrations due to both the decrease in

nitrification activity under non-bloom conditions and the consumption of available nitrate during the bloom.

The inner station was close enough to the glacier front that it was likely affected by the glacially-derived nutrients. The bloom we recorded occurred during a singular time, when the mixed and non-stratified water column from pre-bloom winter conditions was disturbed by the first subglacial meltwater input in May. Yet not enough glacial ice was melting that could generate osmotic stress and prevent cell growth. Simultaneously not enough particulate material was discharged to diminish light penetration and limit photosynthesis. Besides, subglacial discharge induced the upwelling of nutrients (Lydersen et al. 2014). The supply of nitrate and silicate to concentrations up to 9.05 and 2.80 µmol/L respectively (Table 3) likely triggered the marine production and stimulated the diatom bloom. This may explain the diatom dominance (> 98%, Fig 5) and the higher Chl*a* values at the inner fjord compared to the outer fjord (Table 3), unlike previous studies (e.g. Hodal et al. 2012, Hegseth and Tverberg 2013, Piquet et al. 2014). A recent study, also performed during 2012 in Kongsfjorden (Bazzano et al. 2014), revealed the glacial delivery of trace elements, such as potentially bioavailable iron that could have further supported primary productivity during the bloom. A more detailed analysis of fjord and glacial water mass distributions and circulation would be necessary in order to quantify the mechanisms and specific contributions of the different types of meltwater influencing the nutrient fluxes and bloom dynamics in the fjord system (Beaird et al. 2015).

Total cell abundance during the bloom revealed an outstanding contribution of diatoms over the entire fjord (Fig.5), peaking in the upper layer of the inner and middle fjord (Table 3). The associated increase in biogenic silicate and decrease in inorganic silicate with higher values of diatom cells attested to the incorporation of inorganic silicate into opal frustules of diatoms. The

bloom was dominated by genera *Chaetoceros*, *Thalassiosira* and *Fragilaria* (data not shown), commonly found and already reported in high latitude blooms (e.g. Hodal et al. 2012; Hegseth and Tverberg 2013). Consecutive low phytoplankton biomass periods, August and October, were dominated by cryptophytes (e.g. *Cryptomonas spp*.), dinoflagellates (e.g. *Gymnodinium spp.)* and nanoflagellates (Fig. 5), with total cell abundances increasing towards the outer fjord. Hence there was a seasonal variation from large to small cells, simultaneous with the intrusion of Atlantic waters and the increase in water column temperature (Fig. 4), especially in the middle and outer fjord. Few cells of *Cryptomonas* and *Gymnodinium*, have been previously reported, during the summer season, on the western Svalbard shelf (Owrid et al. 2000) and in freshwaters in the vicinity of Ny-Ålesund (Kim et al. 2011).

The increase in Si:N ratios, from a minimum value of 0.1 in May to a maximum of 0.7 in the summer and fall, may explain the shift from diatom cells to smaller and non-siliceous phytoplankton cells (Egge and Aksnes 1992). The significant increase in Si:N ratios with decreasing salinity is consistent with a coupling between silicate availability and glacier run off. The post-bloom conditions in August (with a strong decrease in air temperature and PAR, Fig. 2) were characterized by large sub-glacial discharge from the inner tidewater glaciers, contributing to the decrease in salinity in surface waters (Fig. 3 and Fig. 4) and to high sediment fluxes (max. 300 g m^2 d^{-1} in August, Lalande et al. 2016). The concomitant rise in water column turbidity and stratification resulted in a decrease in light availability and increased in osmotic stress, drastically reducing phytoplankton biomass and leading to very low Chl*a* values (0.04-0.52 µg L^{-1}) (Table 3, Fig. 4). Accordingly, high contributions of pheopigments relative to Chl*a* after the bloom were observed, with ratios close to one, indicating that most of the present phytoplanktonic biomass was degraded, probably due to both pigment digestion by active

zooplankton grazers (Lalande et al. 2016) and algal cell senescense under poor nutrient conditions.

4.2. Nature and origin of total suspended material and particulate organic carbon

The concentration of total suspended material (TSM) in Kongsfjorden is well known to be mainly a reflection of the glacier activity, which brings meltwaters and inorganic particles into the fjord (Beszczyńska-Møller et al. 1997). Accordingly, TSM decreased whith increasing the distance from the glacier front (R^2=0.27, P<0.01). The highest concentrations of TSM were observed in surface waters of the inner and middle part of the fjord during May, reaching a peak of more than 12 mg/L of TSM at the inner fjord, similar to values previously observed in Kongsfjorden during spring (Svendsen et al. 2002). As glacial meltwater was highest during August and October, according to hydrography data, it is strange that we found the highest TSM values in May. We believe that this was due to sampling constraints since water sampling was performed using niskin bottles that allowed for the collection of surface waters only from 2-3 meters depth, likely underestimating the turbid fresh water layer, low in density, that spread into the fjord within the upper 0-2 meters. Another explanation could be a seasonal transition from a distributed to a channelized subglacial drainage system (Bathia et al. 2013). Through the seasons, the suspended material in the whole fjord basin, both at the upper and bottom layer, was mainly composed of lithogenous inorganic particles (~ 90 %) eroded by glaciers and discharged by melting freshwaters. The percentage of POC in TSM ranged between 1 and 12%, gradually increasing when moving away from the glacier front (Table 4).

Changes in POC values during the bloom were strongly dominated by changes in Chl*a* concentration (see section 3.5.). This is consistent with most of the organic material being

composed by fresh cells. However, during August and October the relationship between POC and Chl*a* was much weaker, indicating that sources other than phytoplankton biomass were contributing to the production or delivery of POC during summer and fall. To better understand the origin and nature of this material, isotopic signatures and their relationships with biotic and environmental variables were examined. The high $\delta^{13}C$ values of POC during the bloom at the upper layer of the inner and middle stations (Table 4) is consistent with a marine autochthonous material supplied through primary production at the surface layers of the fjord. Accordingly, $\delta^{13}C$ was significantly positively correlated with Chl*a* during the spring season (Fig. 6, left panel), with the highest value of -22.7‰ occurring at the peak of Chl*a* concentration, which is consistent with phytoplankton end-members commonly used (Schubert and Calvert 2001, Winkelman and Knies 2005). Also during the bloom $\delta^{15}N$-PTN values (ranging from -4.2 to 0.6 ‰), concomitantly with Chl*a*, decreased with increasing nitrate concentrations (Fig. 7, left panel). As phytoplankton tend to preferentially use light ^{14}N-NO_3, such low $\delta^{15}N$ ratios could only be found in nitrate-rich waters, such as those sampled in this study. Accordingly $\delta^{15}N$ co-varied with $\delta^{13}C$ (Fig. 7, right panel), as a consequence of the phytoplankton bloom and the concomitant use of nitrate. During the post-bloom (August and October) $\delta^{13}C$ values were consistently depleted in ^{13}C (ranging from -25.6 to -27.1 ‰) and strongly correlated with salinity (Fig. 6, right panel) indicating the signature of ^{13}C-depleted POC material in fresher waters. This indicates an input of terrigenous POC material coming from the turbid plumes of melting glacial ice. Pelagic Arctic $\delta^{13}C$-POC generally ranges between -26.5 and -22.0‰ (Schubert and Calvert 2001, McMahon et al. 2006, Søreide et al. 2006, Tamelander et al. 2006a), which is similar to the range of values observed during May (with the exception of the deep waters of the outer fjord). However, very low $\delta^{13}C$ signatures and high seasonal variability (-30.5 ‰ in summer and -26.2

‰ in winter) have been previously documented in POC samples from Kongsfjorden by Kędra et al. (2012) with no clear explanation on the origin of these ^{13}C depleted material.

We examine other water column processes that may shed light on the origin of this ^{13}C depleted material present during all seasons, but especially during August and October. Copepods play an important role in the Arctic food web and they are especially adapted to melt influenced environments (Hop et al. 2011). However, they are characterized by ^{13}C values ranging from -23.3 to -22.7 ‰ (Søreide et al. 2006; Tamelander et al. 2006b), which are far from the $\delta^{13}C$-depleted POC values found in August and October. Surface water concentrations of dissolved CO_2, largely controlled by seawater temperature could also be affecting $\delta^{13}C$ values of POC. In accordance with Rau et al. (1989, 1991) who found a negative correlation between the $\delta^{13}C$-POC and water CO_2 concentration, and a positive correlation with water temperature, we may expect lower $\delta^{13}C$ values in POC in winter or in cold seasons compared to summer. However, the trend observed in this study follows the inverse pattern with higher $\delta^{13}C$ values during spring (when water temperature is lower) and lower values during summer and fall (when water temperature increases). Thus neither copepods nor surface CO_2 concentrations can account for the depleted ^{13}C-POC signature observed during August and October.

Terrestrial C_3-plants are also well-known to be relatively more depleted in ^{13}C. Kuliński et al. (2014) recently reported $\delta^{13}C$ values ranging from -35 ‰ to -24.9 ‰ for the terrestrial organic matter of Kongsfjorden, mostly originating from soils, mosses and debris of land vegetation. The supply of this terrestrial material into the fjord waters has never been considered very important at Kongsfjorden as vegetation surface and biomass are scarce. However, the results observed from changes in absorbance spectral slopes, effective tracers for the chemical characteristics and origin of dissolved organic matter, suggest that terrestrial sources might be more important than

previously believed. Low S_R (1.7) and high $S_{350-400}$ (19.3 μm^{-1}) values found at lower salinities (31.8) are indicative of a bigger contribution of high molecular weight organic compounds more common in terrigenous than marine material (Helms et al. 2008), and provide evidence of the input of continental organic matter during the ice melting. Accordingly, more negative ^{13}C-POC values concur with higher $S_{350-400}$ and lower S_R. At the same time $SUVA_{254}$ values, a proxy to estimate the dissolved aromatic carbon content in aquatic systems (Weishaar et al. 2003), were higher at lower salinities and more depleted ^{13}C-POC values, suggesting an input of dissolved aromatics with terrestrial material discharge from glaciers. Interestingly, Grzesiak and co-workers (2015) recently reported an increase in the aromaticity of DOC sampled at the surface of two Svalbard glaciers. Another plausible explanation for the ^{13}C-depleted values is the supply of organic matter from eroded rocks and discharged with the melting freshwaters in summer, and the occurrence of supra-glacial cryoconites that are also discharged into the fjord during the melting seasons. The latter are granular sediment particles that accumulate on glacier surfaces and are composed of mineral and biological material (Anesio and Laybourn-Parry 2012, Cook et al. 2016). Although these structures are poorly understood, they have been identified as hotspots for microbial activity (Edwards et al. 2011, Grzesiak et al. 2015). Recent work (Musilova et al. 2015) has revealed the inputs of microbes and organic matter through eolian transport and snow to cryoconite holes at the Greenland ice sheet, with low δ^{13}C values (from -28 to -27 ‰), very similar to the lower values identified in our study (Table 4, Fig. 6). Thus, the relatively depleted ^{13}C values reported here provide ample evidence of an important and previously overlooked continental source of organic matterial (e.g. land vegetation, eroded lithogenous material and/or debris-enriched cryoconites) directly related with glacier run off. Our findings may also explain the singular ^{13}C depleted organic matter previously reported during a summer season (Kedra et

al. 2012). The primary origin of this organic carbon prior to being transported by the glacier still remains unresolved.

The cryoconite hypothesis may in turn explain the consistently low δ^{15}N-PTN values recorded, averaging 0.7 ‰ (± 1.4 SD) during summer and fall. Indeed, nitrogen fixation (with values close to 0‰) has been recently documented in cryoconite holes on Svalbard glaciers (Telling et al. 2011) and identified as an important process for supporting microbial growth in the middle to late melt season, when concentrations of inorganic nitrogen are depleted. To date, more studies have also found evidence of nitrogen fixation on Arctic glacier microbial aggregates (e.g. Telling et al. 2012, 2014, Segawa et al. 2014). δ^{15}N -PTN values around 0‰ were also found by Kedra et al. (2012) in shallow areas of Kongsfjorden exposed to freshwater loads from melting glaciers.

4.3. Coupling between biopolymeric carbon fractions and phytoplankton population changes

The negative and significant correlation of BP-C (%) with C:N molar ratios identified the BP-C fraction as a good proxy for labile particulate organic matter, where higher proportions of BP-C resulted in organic matter enriched in N, as in Fabiano et al. (1993). The site most affected by seasonal changes in the BP-C fraction was the upper layer at the inner fjord that was, in turn, particularly influenced by high flows of ^{13}C-depleted POC and lithogenous material released by melting glaciers. BP-C fraction at the glacier front peaked to 84.8% in October, with C:N ratios around 3 (Table 4). This latter observation indicates that, even though there was very low primary production and very low POC values in the glacier front during the fall, most of the POC displayed a labile character. This is in accordance with the observed increase in total cell abundance during fall compared to August, especially in the upper water layer of the inner fjord (Table 3). The lower freshwater discharge and hence lower turbidity in the fjord during October,

compared to August, may have increased light penetration. This, together with the slight increase in nutrients in the upper layer (NO^3-, NO^{2-} and PO_4^{3-}, Table 2) may have stimulated a subtle production, not enough to create a bloom, because nutrient concentrations were still low, but sufficient to provide a small amount of fresh biomass. The increase in dinoflagellates, nanoflagellates and cryptophytes during fall (Fig. 5), suggest these phytoplankton groups are well adapted to low nutrient concentrations (NO_3^- < 2.2 µmol/L) and light conditions (PAR< 6 W/m^2).

The dominance of carbohydrates and proteins during the spring bloom (Table 4, Fig. 8), and the strong correlation between PRT content and diatom cell abundance suggests protein-rich cytosol material associated with diatom cells. This is consistent with the presence of extracellular proteins that have been reported from diatom-rich waters in the Antarctic (Raymond et al. 1994). After the bloom in May a seasonal increase in the percentage of lipids coupled with a decrease of both proteins and carbohydrates was observed at all stations (Fig. 8). The pigment ratio (Chl*a*/Pheo ~1) in the upper layers during summer and fall (Table 3) revealed significant grazing pressure and/or diatom cell senescence conditions. These results, alongside observations of sinking diatoms and a shift in phytoplankton community composition (diatoms were replaced by a combination of dinoflagellates, nanoflagellates and cryptophytes), may have induced a shift in the composition of the biopolymeric classes, as lipids reached its highest relative content (more than 80% of BP-C) during the fall compared to values in spring (~40%) and summer (~50 % respectively) (Fig. 8). The significant positive relationship between the percentage of LIP and the relative abundance of cryptophytes suggests that this group may be playing a particularly important role on the stock of lipids in the fjord. Understanding the dynamics on the lipid reserves in the pelagic realm is important as available lipids are valuable high energy food for

Arctic zooplankton (Falk-Petersen et al. 1990) that transfers energy upwards in the marine food web to fish, sea birds and mammals foraging at the tidewater glacier fronts (Lydersen et al. 2013).

4.4. Concluding remarks and implications for climate change

We documented a massive diatom bloom in the glacier front of the inner fjord during spring-time 2012 with Chl*a* concentrations reaching values as high as 15.5 µg/L. These observations stand in contrast to previous studies, which have documented blooms in the middle and/or the mouth of the fjord (e.g. Hegseth and Tverberg 2013). The combination of weak stratification, light availability, and input of nutrients via glacial melt may have induced and favored this short and intense biological production next to the glacier front. The observed bloom represents the most favorable scenario for sustaining, on a seasonal scale, both pelagic (copepods, mammals and seabirds) and benthic life, especially at the glacier front, further fueling ecosystem functioning. The seasonal and spatial patterns observed in this study stand in contrast to previous work, which have highlighted the high variability associated with bloom timing, intensity and phytoplankton community composition. Warming is having an unprecedent impact on both Atlantic water intrusion and glacier retreat, the combination of which are strongly affecting different water properties (i.e. water stratification, turbidity, nutrient concentrations) with consequences for bloom patterns and dynamics. Our results point to the importance of considering not only the consequences of Atlantic Water fluxes on phytoplankton bloom dynamics, but also the impact of glacial melt on fjord nutrient concentrations. A more intense seasonal research effort is needed across Kongsfjorden to better constrain the main critical environmental, hydrological and geochemical factors driving the phytoplankton bloom.

Our results demonstrated how the seasonal release of glacial melt supplied large amounts of lithogenous material, concomitant with small amounts of organic material, that are mostly deposited in the vicinity of the glacier front and partly exported to the mouth of the fjord (Bourgeois et al. 2016). The isotopic composition of the POC present during glacier discharge displays a clear continental signature. Besides ground rocks, the presence of cryoconites and terrestrial organic matter deposited at the surface of the glacier could be an important source of organic nutrients and biogenic organic carbon transported into the fjord with the supra-glacial melting freshwater. However, glacial input of organic continental material in the numerous Arctic fjords, such as Kongsfjorden in Svalbard, have previously been considered of secondary importance and have rarely been studied (Svendsen et al. 2002). As cryoconites has been recently recognized as an important component of the glacier and ice sheet biome, (e.g. Anesio and Laybourn-Parry 2012), ecological and biogeochemical consequences of organic material delivery to fjords and adjacent waters still needs to be explored.

The mass balance for Svalbard glaciers is currently negative and climate change predictions suggest continued warming that will enhance glacial retreat, snow melting and glacial river flows. Recent work highlighted the importance of increased glacial meltwater input, including delivery of essential nutrients and dissolved and particulate organic matter to the polar oceans (Lawson et al. 2014, Hawkings et al. 2015). This may have consequences for bloom dynamics, as well as provoke an increase of continental organic matter discharge. If blooms are intensified with glacier melting it would provide an important negative climate feedback through its effect on marine primary production and CO_2 drawdown (Meire et al. 2015). Furthermore, glacial meltwater discharge in high Arctic fjords has been identifed as an important organic carbon input to the marine system and burial into sediments (Smith et al. 2015). However, the supply of labile

dissolved organic matter that could be respired by heterotrophic bacteria could counteract the CO_2 drawdown. Thus we encourage future investigations to focus on the impacts of inputs from glaciers on bloom dynamics, biogeochemistry and ecology of Arctic fjords and surrounding waters. Ideally, future investigations in the Arctic will also overcome the gap between small-scale (glacier front) / high-resolution (monthly), and large-scale (continental margin) / low-resolution (annual) studies.

Acknowledgments

This research was part of the ECOTAB project funded by The French "Agence Nationale de la Recherche" (Ref: ANR-11-PDOC-0018) and the French Polar Institut Paul Emile Victor (IPEV). We thank the crew of the workboat MS Teistein and the Kings Bay personnel. We also thank Marion Maturilli and all AWIPEV personnel at Ny-Ålesund for dedicated, professional assistance and for providing meteorological data. We thank F. Narcy, J. Richard, E. Amice, A. Aubert, and G. Duong for their help on the field for samples collection and M. LeGoff, R. Corvaisier and B. Beker for nutrient and phytoplankton analyses. We also want to thank the anonymous reviewers who contributed a significant amount of effort to improving the manuscript. M. Ll. C. was funded by the Spanish Research Council, Consejo Superior de Investigaciones Cientificas (CSIC, grant JAEDOC030-2010) and co-funded by the Fondo Social Europeo (FSO). S.B was funded by the Conseil Général du Finistère (CG29). M. K. was further financed by Polish Ministry of Science and Higher Education grant number W70/ECOTAB/2014. We thank J. A. Hale for English corrections and constructive comments.

References

Aminot A, Kérouel R (2007) Dosage automatique des nutriments dans les eaux marines: methodes en flux continu.Quae, France.

Anesio AM, Laybourn-Parry J (2012) Glaciers and ice sheets as a biome. Trends Ecol Evol 27:219-225.

Bathia MP, Das SB, Xu L, Charette MA, Wadham JL, Kujawinski EB (2013) Organic carbon export from the Greenland ice sheet. Geochim Cosmochim Acta 109:329-344

Barnes H, Blackstock J (1973) Estimation of lipids in marine animals and tissues: detailed investigation of the sulphophosphovanilin method for 'total' lipids. J Exp Mar Biol Ecol 12:103-118

Bazzano A, Rivaro P, Soggia F, Ardini F, Grotti M (2014) Anthropogenic and natural sources of particulate trace elements in the coastal marine environment of Kongsfjorden, Svalbard. Mar Chem 163: 28-35

Beaird N, Straneo F, Jenkins W (2015) Spreading of Greenland meltwaters in the ocean revealed by noble gases. Geophys Res Lett 42:7705 – 7713, doi:10.1002/2015GL065003

Beszczyeska-Møller A, Weslawski JM, Walczowski W, Zajaczkowski M (1997) Estimation of glacial meltwater discharge into Svalbard coastal waters. Oceanologia 39:289–298

Bourgeois S, Kerhervé P, Calleja MLl, Many G, Morata N (2016) Glacier inputs influence organic matter composition and prokaryotic distribution in a high Arctic fjord (Kongsfjorden, Svalbard). J Marine Syst 164:112-127

Bradford MM (1976) Rapid and sensitive method for the quantitation of microgram quantities of protein utilizing the principle of protein-dye binding. Anal. Biochem. 72:248–254

Brink RH, Dubach P, Lynch DL (1960) Measurement of carbohydrates in soil hydrolyzates with anthrone. Soil Sci 89:157-166

Cokelet ED, Tervalon N, Bellingham JG (2008) Hydrography of the West Spitsbergen Current, Svalbard Branch: Autumn 2001. J Geophys Res 113, C01006, doi:10.1029/2007JC004150.

Conway JI, Parker EM, Yaguchi M, Mellinger DL (1977) Biological utilization and regeneration of silicon in Lake Michigan. J.Fish Res Board Can 34:537-544

Cook J, Edwards A, Takeuchi N, Irvine-Fynn T (2016) Cryoconite: The dark biological secret of the cryosphere. Progress in Phys Geogr 40 (1) : 66-111, DOI: 10.1177/0309133315616574

Cottier F, Tverberg V, Inall M, Svendsen H, Nilsen F, Griffiths C (2005) Water mass modification in an Arctic fjord through cross- shelf exchange: the seasonal hydrography of Kongsfjorden, Svalbard. J Geophys Res-Oceans 110:1–18. doi:10.1029/2004 jc002757

Cottier FR, Nilsen F, Inall ME, Gerland S, Tverberg V, Svendsen H (2007) Wintertime warming of an Arctic shelf in response to large-scale atmospheric circulation. Geophys Res Lett 34, L10607, doi: 10.1029/2007gl029948

Danovaro R, Dell'Anno A, Fabiano M (2001) Bioavailability of organic matter in the sediments of the Porcupine Abyssal Plain, northeast Atlantic. Mar Ecol Progr Ser 220:25-32

Doney SC, Ruckelshaus M, Duffy JE, Barry JP, Chan F, English CA, Galindo HM, Grebmeier JM, Hollowed AB, Knowlton N, Polovina J, Rabalais NN, Sydeman WJ, Talleyet LD (2012)

Climate Change Impacts on Marine Ecosystems. Ann Rev of Mar Sci (4):11-37. DOI: 10.1146/annurev-marine-041911-111611

Dreywood R (1946) Qualitative test for carbohydrate material. Ind Eng Chem Anal Ed 18: 499-499. DOI: 10.1021/i560156a015

Edwards A, Anesio AM, Rassner SM, Sattler B, Hubbard B, Perkins W T, Young M, Griffith, GW (2011) Possible interactions between bacterial diversity, microbial activity and supraglacial hydrology of cryoconite holes in Svalbard. ISME J, 5(1), 150–160. http://doi.org/10.1038/ismej.2010.100

Egge JK and Aksnes DL (1992) Silicate as regulating nutrient in phytoplankton competition. Mar Ecol Prog Ser 83:281–289

Eilertsen HC, Taasen JP, Weslawski JM (1989) Phyto- plankton studies in the fjords of West Spitsbergen: physical environment and production in spring and summer. J Plankton Res 11:245–1260

Fabiano M, Povero P, Danovaro R (1993) Distribution and composition of particulate organic matter in the Ross Sea (Ant- arctica). Polar Biol 13: 525-533

Falk-Petersen S, Sargent JR, Hopkins CCE (1990) Trophic relationships in the pelagic arctic food web. In: Barnes M and Gibson RN (eds), Trophic Relationships in the Marine Environment. Scotl. Univ. Press, Aberdeen, pp. 315–333.

Førland EJ, Benestad R, Hanssen-Bauer I, Hauge JE, Skaugen TE (2011) Temperature and Precipitation Development at Svalbard 1900–2100. Adv Meteor, doi:10.1155/2011/893790

Frankowski M, ZIola-Frankowska A (2014) Analysis of labile form of aluminum and heavy metals in bottom sediments from Kongsfjord, Isfjord, Hornsund fjords. Environ Earth Sci 71:1147-1158. doi: 10.1007/s12665-013-2518-5

Grannas AM, Jones AE, Dibb J, Ammann M, Anastasio C, Beine H, Bergin M, Bottenheim J, Boxe CS, Carver G, Crawford JH, Domine F, Frey MM, Guzman MI, Heard D, Helmig D, Hoffmann MR, Honrath R E, Huey LG, Jacobi H-W, Klan P, McConnell J, Sander R, Savarino J, Shepson PB, Simpson WR, Sodeau J, von Glasgow R, Weller R, Wolff E, Zhu T (2007). An overview of snow photochemistry: evidence, mechanisms and impacts. Atmos Chem and Phys 7: 4329–4373

Grannas AM (2014) Chemical Composition of Snow, Ice and Glaciers. In: Singh V, Singh P and Haritashya UK (eds), Encyclopedia of Snow, Ice and Glaciers. Springer Netherlands, pp. 133-135. DOI: 10.1007/978-90-481-2642-2_59

Grebmeier JM, Cooper LW, Feder HM, Sirenko BI (2006) Ecosystem dynamics of the Pacific-influenced Northern Bering and Chukchi Seas in the Amerasian Arctic. Prog Oceanogr 71:331–361. doi: 10.1016/j.pocean.2006.10.001

Grotti M, Soggia F, Ianni C, Magi E, Udisti R (2013) Bioavailability of trace elements in surface sediments from Kongsfjorden, Svalbard. Mar Pollut Bull 77:367-374. doi: 10.1016/j.marpolbul.2013.10.010

Grzesiak J, Górniak D, Świątecki A, Aleksandrzak-Piekarczyk T, Szatraj K, Zdanowski MK (2015) Microbial community development on the surface of Hans and Werenskiold Glaciers

(Svalbard, Arctic): a comparison. Extremophiles 19(5): 885-897. doi:10.1007/s00792-015-0764-z.

Hanelt D, Bischof K, Wiencke C (2001) The radiation, temperature and salinity regime in Kongsfjorden. In: Wiencke C (ed) The coastal ecosystem of Kongsfjorden, Svalbard. Synopsis of biological research performed at the Koldewey Station in the years 1991-2003 AWIPEV, Bremerhaven, Germany

Hansen BB, Isaksen K, Benestad RE, Kohler J, Pedersen ÅØ, Loe LE, Coulson SJ, Larsen JO, Varpe Ø (2014) Warmer and wetter winters: characteristics and implications of an extreme weather event in the High Arctic, Environ Res Lett 9:114021, doi:10.1088/1748-9326/9/11/114021

Hawkings JR, Wadham JL, Tranter M, Lawson E, Sole A, Cowton T, Tedstone AJ, Bartholomew I, Nienow P, Chandler D, Telling J (2015) The effect of warming climate on nutrient and solute export from the Greenland Ice Sheet. Geochem Persp Let. I, 94-104. doi: 10.7185/geochemlet.1510

Hegseth EN, Tverberg V (2008) Changed spring bloom timing in a Svalbard (high Arctic) fjord caused by Atlantic water inflow? Paper presented at the SCAR conference 'polar research-arctic and antarctic perspectives in the international polar year', St. Petersburg, 7–11 July 2008

Hegseth EN, Tverberg V (2013) Effect of Atlantic water inflow on timing of the phytoplankton spring bloom in a high Arctic fjord (Kongsfjorden, Svalbard). J Marine Syst 113:94-105

Hillebrand H, Durselen CD, Kirschtel D, Pollingher U, Zohary T (1999) Biovolume calculation for pelagic and benthic microalgae. J Phycol 35, 403–424

Hodal H, Falk-Petersen S, Hop H, Kristiansen S, Reigstad M (2012) Spring bloom dynamics in Kongsfjorden, Svalbard: nutrients, phytoplankton, protozoans and primary production. Polar Biol 35:191–203. doi:10.1007/s00300-011-1053-7

Holte B, Dahle S, Gulliksen B, Naes K (1996) Some macrofaunal effects of local pollution and glacier-induced sedimentation, with indicative chemical analyses, in the sediments of two Arctic fjords. Polar Biol 16:549–557

Holte B, Gulliksen B (1998) Common macrofaunal dominant species in the sediments of some north Norwegian and Svalbard glacial fjords. Polar Biol 19:375–382

Hop H, Pearson T, Hegseth EN, Kovacs KM, Wiencke C, Kwasniewski S, Eiane K, Mehlum F, Gulliksen B, Wlodarska - Kowalczuk M, Lydersen C (2002) The marine ecosystem of Kongsfjorden, Svalbard. Polar Res 21:167– 208

Hop H, Falk-Petersen S, Svendsen H, Kwasniewski S, Pavlov V, Pavlova O, Søreide JE (2006) Physical and biological character- istics of the pelagic system across Fram Strait to Kongsfjorden. Prog Oceanogr 71:182–231. doi:10.1016/j.pocean.2006.09.007

Hop H, Mundy CJ, Gosselin M Rossnagel AL, Barber DG (2011) Zooplankton boom and ice amphipod bust below melting sea ice in the Amundsen Gulf, Arctic Canada. Polar Biol 34: 1947. doi:10.1007/s00300-011-0991-4

Hood E, Battin TJ, Fellman J, O'Neel S, Spencer RGM (2015) Storage and release of organic carbon from glaciers and ice sheets. Nature Geos 8:91-96, doi:10.1038/ngeo2331

Ito H, Kudoh S (1997) Characteristics of water in Kongsfjorden, Svalbard. Proc. NIPR Symp Polar Meteorol Glaciol 11:211-232

Iversen KR, Seuthe L (2011) Seasonal microbial processes in a high-latitude fjord (Kongsfjorden, Svalbard): I. Heterotrophic bacteria, picoplankton and nanoflagellates. Polar Biol 34:731-749. doi:10.1007/s00300-010-0929-2

Kędra M, Kulinski K, Walkusz W, Legezynska J (2012) The shallow benthic food web structure in the high Arctic does not follow seasonal changes in the surrounding environment. Estuar Coast Shelf S 114:183-191.

Kedra M, Moritz M, Choy ES, David C, Degen R, Duerksen S, Ellingsen I, Górska B, Grebmeier JM, Kirievskaya D, Oevelen DV, Piwosz K, Samuelsen A, Węsławsk JM (2015) Status and trends in the structure of Arctic benthic food webs. Polar Research 34, 23775, http://dx.doi.org/10.3402/polar.v34.23775

Kim, JH, Peterse F, Willmott V Kristensen DK, Baas M, Schouten S, Sinninghe Damsté JS (2011) Large ancient organic matter contributions to Arctic marine sédiments (Svalbard). Limnol Oceanogr 56:1463-1474

Kortsch S, Primicerio R, Beuchel F, Renaud PE, Rodrigues J, Lønne OJ, Gullikse B (2012) Climate-driven regime shifts in Arctic marine benthos. PNAS 109 (35): 14052-14057. doi/10.1073/pnas.1207509109

Krishfield RA, Proshutinsky A, Tateyama K, Williams WJ, Carmack EC, McLaughlin FA, Timmermans ML (2014) Deterioration of perennial sea ice in the Beaufort Gyre from 2003 to

2012 and its impact on the oceanic freshwater cycle. J Geophys Res: Oceans. doi: 10.1002/2013JC008999

Kubiszyn AN, Piwosz K, Wicktor JM Jr, Wicktor JM (2014) The effect of inter-annual Atlantic water inflow variability on the planktonic protist community structure in the West Spitsbergen waters during the summer. J Plankton Res 0(0): 1–14. doi:10.1093/plankt/fbu044

Kulinski K, Kedra M, Legezynska J, Gluchowska M, Zaborska A (2014) Particulate organic matter sinks and sources in high Arctic fjord, J Marine Syst doi: 10.1016/j.jmarsys.2014.04.018

Lalande C, Moriceau B, Leynaert A, Morata N (2016) Spatial and temporal variability in export fluxes of biogenic matter in Kongsfjorden. Polar Biol DOI 10.1007/s00300-016-1903-4

Lang C, Fettweis X, Erpicum M (2015) Future climate and surface mass balance of Svalbard glaciers in an RCP8.5 climate scenario: a study with the regional climate model MAR forced by MIROC5. The Cryosphere 9: 945–956, doi:10.5194/tc-9-945-2015

Lawson EC, Bhatia MP, Wadham JL, Kujawinski EB (2014) Continuous summer export of nitrogen-rich organic matter from the Greenland Ice Sheet inferred by ultra high resolution mass spectrometry. Environ Sci Technol 48, 14248-14257.

Lefauconnier B, Hagen JO, Rudant JP (1994) Flow speed and calving rate of Kongsbreen glacier using SPOT images. In Spjelkavik S (ed): Proceedings of the Second Circumpolar Symposium on Remote Sensing of Arctic Environments, Tromsø, Polar Res 13:59–65

Leu E, Falk-Petersen S, Kwasniewski S, Wulff A, Edvardsen K, Hessen DO (2006) Fatty acid dynamics during the spring bloom in a High Arctic fjord: importance of abiotic factors versus community changes. Can J Fish Aquat Sci 63:2760–2779. doi:10.1139/f06-159

Lydersen C, Assmy P, Falk-Petersen S Kohler J, Kovacs KM, Reigstad M, Steen H, Strøm H, Sundfjord A, Varpe Ø, Walczowski W (2014) The importance of tidewater glaciers for marine mammals and seabirds in Svalbard, Norway. J Marine Syst 129:452–471. doi:10.1016/j.jmarsys.2013.09.006

Meehl GA, Covey C, Delworth T, Latif M, McAvaney B, Mitchell JFB (2007) The WCRP CMIP3 multimodel dataset: a new era in climatic change research. Bull of the Am Meteorol Soc 88(9):1383–1394.

Meire L, Søgaard DH, Mortensen J, Meysman FJR, Soetaert K, Arendt KE, Juul-Pedersen T Blicher ME, Rysgaard S (2015) Glacial meltwater and primary production are drivers of strong CO2 uptake in fjord and coastal waters adjacent to the Greenland Ice Sheet. Biogeosciences 12: 2347–2363, doi:10.5194/bg-12-2347-2015

MacLachlan SE, Cottier FR, Austin WEN, Howe JA (2007) The salinity: $d^{18}O$ water relationship in Kongsfjorden, western Spitsbergen. Polar Res. 26:160–167. doi: 10.1111/j.1751-8369.2007.00016.x

McMahon K, Ambrose WG Jr, Johnson BJ, Sun MY, Lopez GR, Clough LM, Carrol ML (2006) Benthic community response to ice algae and phytoplankton in Ny Ålesund, Svalbard. Mar Ecol Prog Ser 310: 1–14

Musilova M, Tranter M, Bennett SA, Wadham J, Anesio AM (2015) Stable microbial community composition on the Greenland Ice Sheet. Frontiers in Microbiol doi: 10.3389/fmicb.2015.00193

Owrid G, Socal G, Civitarese G Luchetta A, Wiktor J, Nöthig EM, Andreassen I, Schauer U, Strass V (2000) Spatial variability of phytoplankton, nutrients and new production estimates in the waters around Svalbard. Polar Res 19:155–171. doi:10.1111/j.1751-8369.2000.tb00340.x

Paasche E (1980) Silicon content of 5 marine plankton diatom species measured with a rapid filter method. Limnol Oceanogr 25:474–480

Parsons TR, Maita Y, Lalli CM (1984) A manual of chemical and biological methods for seawater analysis. Pergamon Press, Oxford

Piechura J, Walczowski W (2009) Warming of the West Spitsbergen Current and sea ice north of Svalbard, Oceanologia, 51(2), pp 149-164

Piquet AMT, van de Poll WH, Visser RJW, Wiencke C, Bolhuis H, Buma AGJ (2014) Springtime phytoplankton dynamics in Arctic Krossfjorden and Kongsfjorden (Spitsbergen) as a function of glacier proximity. Biogeosciences, 11, 2263–2279. doi:10.5194/bg-11-2263-2014

Piwosz K, Walkusz W, Hapter R, Wieczorek P, Hop H, Wiktor J (2009) Comparison of productivity and phytoplankton in a warm (Kongsfjorden) and a cold (Hornsund) Spitsbergen fjord in mid-summer 2002. Polar Biol 32:549–559. doi:10.1007/s00300-008-0549-2

Polyakov IV, Beszczynska A, Carmack EC, Dmitrenko IA, Fahrbach E, Frolov IE, Gerdes R, Hansen E, Holfort J, Ivanov VV, Johnson MA, Karcher M, Kauker F, Morison J, Orvik KA,

Schauer U, Simmons HL, Skagseth Ø, Sokolov VT, Steele M, Timokhov LA, Walsh D, Walsh JE (2005) One more step toward a warmer Arctic, Geophys Res Lett 32, L17605, doi:10.1029/2005GL023740.

Pritchard HD, Arthern RJ, Vaughan DG, Edwards LA. (2009). Extensive dynamic thinning on the margins of the Greenland and Antarctic ice sheets. Nature 461: 971–975.

Rachlewicz G, Szczuciński W, Ewertowski M (2007) Post− "Little Ice Age" retreat rates of glaciers around Billefjorden in central Spitsbergen, Svalbard. Polish Polar Research 28: 159–186

Ragueneau O, Savoye N, Del Amo Y, Cotten J, Tardiveau B, Leynaert A (2005) A new method for the measurement of biogenic silica in suspended matter of coastal waters using Si:Al ratios to correct for the mineral interference. Cont Shelf Res 25:697–710. doi:10.1016/j.csr.2004.09.017

Raymond JA, Sullivan CW, Devries AL (1994) Release of an ice-active substance by Antarctic seaice diatoms. Polar Biol 14:71-75

Riley GA (1970) Particulate organic matter in sea water. Adv Mar Biol 8:1-118.

Schauer U, Fahrbach E, Osterhus S, Rohardt G (2004) Arctic warming through the Fram Strait: Oceanic heat transport from 3 years of measurements, J Geophys Res 109, C06026, doi:10.1029/2003JC001823.

Schubert CJ, Calvert SE (2001) Nitrogen and carbon isotopic composition of marine and terrestrial organic matter in Arctic Ocean sediments: Implications for nutrient utilization and organic matter composition. Deep-Sea Res PT I 48:789–810. doi:10.1016/S0967-0637(00)00069-8

Schubert CJ, Nielsen B (2000) Effects of decarbonation treatments on delta C-13 values in marine sediments. Mar Chem 76: 55-59

Segawa T, Ishii S, Ohte N, Akiyoshi A, Yamada A, Maruyama F, Li Z, Hongoh Y, Takeuchi N (2014) Environ Microbiol 16(10): 3250-62. doi: 10.1111/1462-2920.12543.

Skirbekk K, Kristensen DK, Rasmussen TL, Koç N, Forwick M (2010) Holocene climate variations at the entrance to a warm Arctic fjord: evidence from Kongsfjorden trough, Svalbard, in: Fjord Systems and Archives, edited by: Howe, J. A., Austin, W. E. N., Forwick, M., and Paetzel, M., Geological Society of London, Special Publications, 344, London, 289–304.

Smith RW, Bianchi TS, Allison M, Savage C, Galy V (2015) High rates of organic carbon burial in fjord sediments globally. Nature Biogeos 8:450-454, DOI: 10.1038/NGEO2421

Søreide JE, Hop H, Carroll ML, Falk-Petersen S, Hegseth EN (2006) Seasonal food web structures and sympagic–pelagic coupling in the European Arctic revealed by stable isotopes and a two-source food web model. Prog Oceanogr 71: 59–87.

Spencer RGM, Weidong G, Raymond P, Dittmar T, Hood E, Fellman J, Stubbins A (2014) Source and biolability of ancient dissolved organic matter in glacier and lake ecosystems on the Tibetan plateau. Geochim Cosmochim Acta, 142, pp. 64–74 http://dx.doi.org/10.1016/j.gca.2014.08.006

Stroeve JC, Serreze M, Fetterer F, Arbetter T, Meier W, Maslanik J, Knowles K (2005) Tracking the Arctic's shrinking ice cover: another extreme September minimum in 2004. Geophys Res Lett 32(4): L04501.

Stubbins A, Hubbard V, Uher G, Aiken G, Law CS, Upstill-Goddard RC, Mopper K (2008) Relating carbon monoxide photoproduction to dissolved organic matter functionality. Environ Sci Technol 42, 3271–3276.

Svendsen H, Beszczynska-Møller A, Hagen JO, Lefauconnier B, Tverberg V, Gerland S, Ørbøk JB, Bischof K, Papucci C, Zajaczkowski M, Azzolini R (2002) The physical environment of Kongsfjorden– Krossfjorden, an Arctic fjord system in Svalbard. Polar Res 21:133–166

Tamelander T, Renaud PE, Hop H, Carroll ML, Ambrose WG Jr, Hobson KA (2006a). Trophic relationships and pelagic-benthic coupling during summer in the Barents Sea Marginal Ice Zone, revealed by stable carbon and nitrogen isotope measurements. Mar Ecol Prog Ser 310, 33-46.

Tamelander T, Søreide JE, Hop H, Carroll ML (2006b) Fractionation of stable isotopes in the Arctic marine copepod Calanus glacialis: effects on the isotopic composition of marine particulate organic matter. J Exp Marine Biol Ecol 333 (2), 231-240

Telling J, Anesio AM, Tranter M, Irvine-Fynn T, Hodson A, Butler C, Wadham J (2011) Nitrogen fixation on Arctic glaciers, Svalbard. J Geophys Res 116: 1–8 (G03039)

Telling J, Stibal M, Anesio AM, Tranter M, Nias I, Cook J, Lis G, Wadham JL, Sole A, Niewnow P, Hodson A (2012) Microbial nitrogen cycling on the Greenland Ice Sheet. Biogeosciences 9, 2431–2442. doi:10.5194/bg-9-2431-2012

Telling J, Anesio AM, Tranter M, Fountain AG, Nylen T, Hawkings J, Singh VB, Kaur P, Musilova M, Wadham JL (2014) Spring thaw ionic pulses boost nutrient availability and microbial growth in entombed Antarctic Dry Valley cryoconite holes. Front Microbiol 5:694. doi: 10.3389/fmicb.2014.00694

Utermöhl H (1958) Zur Vervollkommnung der quantitativen Phytoplankton-Methodik. Mitt Int Verein Limnol 9: 1-38

Van De Poll Willem H, Maat Douwe S, Fischer Ph, Rozema PD, Daly OB., Koppelle S, Visser RJW, Buma AGJ (2016) Atlantic Advection Driven Changes in Glacial Meltwater: Effects on Phytoplankton Chlorophyll-a and Taxonomic Composition in Kongsfjorden, Spitsbergen, Front Mar Sci 3:200, doi: 10.3389/fmars.2016.00200

Walczowski W (2013) Frontal structures in the West Spitsbergen Current margins, Ocean Sci 9, 957-975, doi:10.5194/os-9-957-2013

Wang GZ, Guo CY, Luo W, Cai MH, He JF (2009) The distribution of picoplankton and nanoplankton in Kongsfjorden, Svalbard during late summer 2006. Polar Biol 32:1233–1238. doi: 10.1007/s00300-009-0666-6

Weishaar JL, Aiken GR, Bergamaschi BA, Fram MS, Fujii R, Mopper K (2003) Evaluation of Specific Ultraviolet Absorbance as an Indicator of the Chemical Composition and Reactivity of Dissolved Organic Carbon. Environ Sci Technol 37 (20): 4702-4708. DOI: 10.1021/es030360x

Welschmeyer NA, Lorenzen CJ (1985) Role of herbivory in controlling phytoplankton abundance – annual pigment budget for a temperate marine fjord. Mar Biol 90:75-86

Winkelman D, Knies J (2005) Recent distribution and accumulation of organic carbon on the continental margin west off Spitsbergen. Geochem Geophy Geosy, Q09012, doi:10.1029/2005GC000916

Wiktor J (1999) Early spring microplankton development under fast ice covered fjords of Svalbard, Arctic. Oceanologia 41:51–72

Włodarska-Kowalczuk M, Pearson TH (2004) Soft-bottom macrobenthic faunal association and factors affecting species distributions in an Arctic glacial fjord (Kongsfjord, Spitsbergen). Polar Biol 27:155-167

Włodarska-Kowalczuk M, Pearson TH, Kendall MA (2005) Benthic response to chronic natural physical disturbance by glacial sedimentation in an Arctic fjord. Mar Ecol Prog Ser 303:31–41

Wynn PM, Hodson AJ, Heaton THE, Chenery SR (2007) Nitrate production beneath a High Arctic Glacier, Svalbard. Chem Geol 244:88-102. doi: 10.1016/j.chemgeo.2007.06.008

Highlights 3-5 bullet points (max 85 characters, including spaces, per bullet point)

- Glacier retreat is affecting the ecosystem dynamics of high arctic fjords
- Seasonal and spatial environmental changes of Kongsfjorden were examined during 2012
- The bloom dynamics and changes in the pelagic geochemistry were evaluated
- A singular and strong diatom bloom was observed in May at the fjord glacier front
- Isotopic data revealed very depleted organic material during high melting seasons